AD-A126 871 SEDIMENTS ON THE SOUTHEASTERN FLANK OF THE BERMUDA PEDESTAL(U) NAVAL OCEAN RESEARCH AND DEVELOPMENT ACTIVITY NSTL STATION MS D LAVOIE ET AL. MAR 83 1/2

UNCLASSIFIED NORDA-TN-198 F/G 8/10 . NL

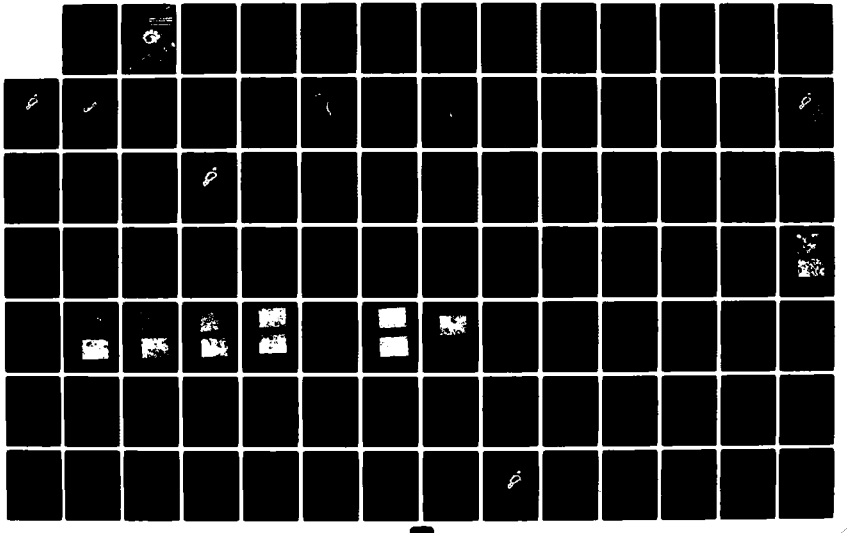

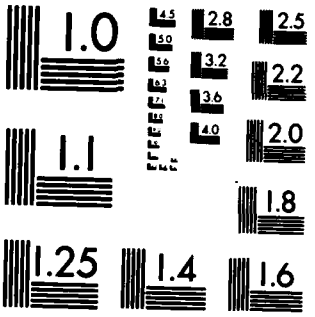

Naval Ocean Research and
Development Activity
NSTL Station, Mississippi 39529

Sediments on the Southeastern Flank of the Bermuda Pedestal

NAVAL OCEAN RESEARCH AND DEVELOPMENT ACTIVITY 1976

ACKNOWLEDGMENTS

We are greatly indebted to Dr. William Ward, University of New Orleans, who provided guidance at critical times during the completion of this work. Dr. Joseph Kelly, also of the University of New Orleans, made many valuable suggestions during the initial stages of planning. Dr. Frederick Bowles of NORDA made available his sediment laboratory during many months of analysis, as well as critically reading the manuscript. Dennis Lavoie of NORDA provided invaluable assistance with the grain size analyses and unraveled the mysteries of the Elzone Counter. Linda McRaney of NORDA provided editorial assistance. Funding was provided by the Naval Electronics Systems Command, Code 612, Bottom Interaction Program (PE 62759N).

TABLE OF CONTENTS

LIST OF FIGURES

LIST OF TABLES

ABSTRACT

The Bermuda Pedestal is a truncated, flat-topped, volcanic cone located in the western North Atlantic Ocean at approximately 32°20'N and 64°45'W. The pedestal has steep slopes ranging from 30° near the top to 2.5° near the bottom. Seismic records indicate sparse sediment cover on the slopes and an absence of large amounts of slump material on the lower slopes of the pedestal. This suggests that the apron at the base is not recent; rather, it may be a remnant of a talus slope associated with mid Eocene-Oligocene volcanic and erosional events.

The carbonate content of surface and near-surface sediment (quaternary) is generally high, decreasing only slightly with increasing depth in spite of probable extensive dissolution. Carbonate constituents are composed of both shallow platform and pelagic organisms. Constituent particles identified by scanning electron microscopy correlate well in most instances with mineralogy identified by X-ray diffraction. Clay mineral content is low to nonexistent on the pedestal. In general, grain sizes tend to be coarser near the top of the pedestal, but anomalously high percentages of sand were found in a few places low on the flank and apron of the pedestal.

Sediment deposition on the pedestal is discontinuous and episodic, a combination of pelagic "rain" and redeposition by rapid-transport processes such as slumping, turbidity currents, and resuspension and dispersion of sediment by eddies and currents.

INTRODUCTION

There has been considerable interest in the geology of Bermuda since the early 1900's. Most of the early sedimentological studies were concerned, of necessity, with the islands of Bermuda. Only with the advent of sophisticated seismic and coring techniques were investigators able to study the surrounding sea floor. Much of the work to date has been concentrated on the Bermuda Rise; some work was done on the apron, but little was done on the pedestal itself.

The objective of this study is to describe the surface sediments on the southeastern flank of the pedestal and to discuss the processes which control their characteristics, with emphasis on providing background for future research related to the Bermuda Pedestal and surrounding areas. Of particular interest are the recent sediment types and thicknesses on the pedestal, the surrounding apron, and the rise. The approach used was to integrate information in the literature concerning surrounding areas together with fresh evaluations of already available data and of new sedimentological analyses. Data for the apron and the rise were gleaned from the literature and ten additional cores analyzed by the U.S. Naval Oceanographic Office (NAVOCEANO). Samples from the top 40 centimeters (cm) of eleven cores taken from the pedestal itself were obtained from Lamont-Doherty Geological Observatory Core Repository and were analyzed to provide primary data on the pedestal.

A detailed bathymetry map was compiled to provide a base for the study. This is a new compilation incorporating (1) the detailed contours (converted to meters) of the Bermuda Pedestal from the U.S. Navy H.O.

16,985 Misc. Chart dated September 1960, (2) the shallow-water reef details from U.S. Navy Chart 26341 dated June 1980, and (3) the contours in the southeastern portions from Bowles (1980). The remainder was contoured from raw track data provided by NAVOCEANO and the National Geophysical and Solar-Terrestrial Data Center (NGSDC) (Appendix 1).

Seismic reflection profiles were examined to provide additional insight into the sediment thickness and patterns on and around the pedestal and apron. The continuous seismic reflection profiles were obtained from Navy files and Lamont-Doherty Geological Observatory (Appendices 3 and 5).

Geologic Setting

The Bermuda Rise, located in the center of the North American Basin is a low, broad, northeast-trending arch 560 kilometers (km) by 1100 km in dimension (Fig. 1). Near the center of the arch lies the Bermuda Pedestal (Figs. 1 and 2), a truncated volcanic cone. About 350 islands occupy 10% of the platform area of roughly 2000 square kilometers (Gees and Medioli, 1970). The islands are clustered on the southeastern edge of the platform. Around the remainder of the platform lie carbonate banks and submerged and lithified dune ridges covered with a thin veneer of coral and algae (Stanley and Swift, 1967, 1968). There are patch reefs of Homotrema, coral and red algae (Jordan, 1971), and red-algal cup reefs (Ginsberg and Schroeder, 1973) known as "boilers," resembling the algal Lithothamnion ridges of Pacific atolls. These cup reefs are located primarily in the southeastern portion of the platform (Fig. 3).

In addition to the islands, banks and reefs, the platform also includes the shallow lagoonal areas within the banks and a broad "reef" front terrace known by fishermen as "broken ground," which extends seaward from the reef to the edge of the platform.

Based on bathymetry (Fig. 2), there is a discernible pattern of slopes on the Bermuda Pedestal. The Bermuda Platform is surrounded by slopes of approximately 30° to depths of 1000 meters (m) to 1500 m. Below this, to a depth of 3000 m, is an intermediate zone that has slopes ranging from 5° to 13°. Below 3000 m is a zone that has slopes between 2.5° and 3.8°, which appears to be a sedimentary apron or deep sea fan. This pattern is broken by Bowditch Seamount, Challenger Bank, and Plantagenet Bank. Bowditch Seamount is a roughly conical-shaped feature 1300 m in height situated about midway down the northeastern side of the Bermuda Pedestal that probably represents a secondary volcanic center or side vent (Fig. 2). This feature has always been submerged. Challenger and Plantagenet Banks, also part of the Bermuda Pedestal, are situated on the southwestern side of the Bermuda Pedestal (Fig. 2). Their slopes average 20° to 22°. These features probably also represent secondary sources of vulcanism and are significantly larger than Bowditch Seamount. These three features seem to have been built on the zones of intermediate and low slopes without the apparent apron at their bases. They have steep slopes all the way to their bases.

Holcombe and Heezen (1970) divided the Bermuda Rise into several provinces based on elevation and slopes of the sea floor. Most of the rise is considered "rough" seafloor with elevations of 96 m to 375 m and slopes ranging between 5° and 15°; the distance between topographic

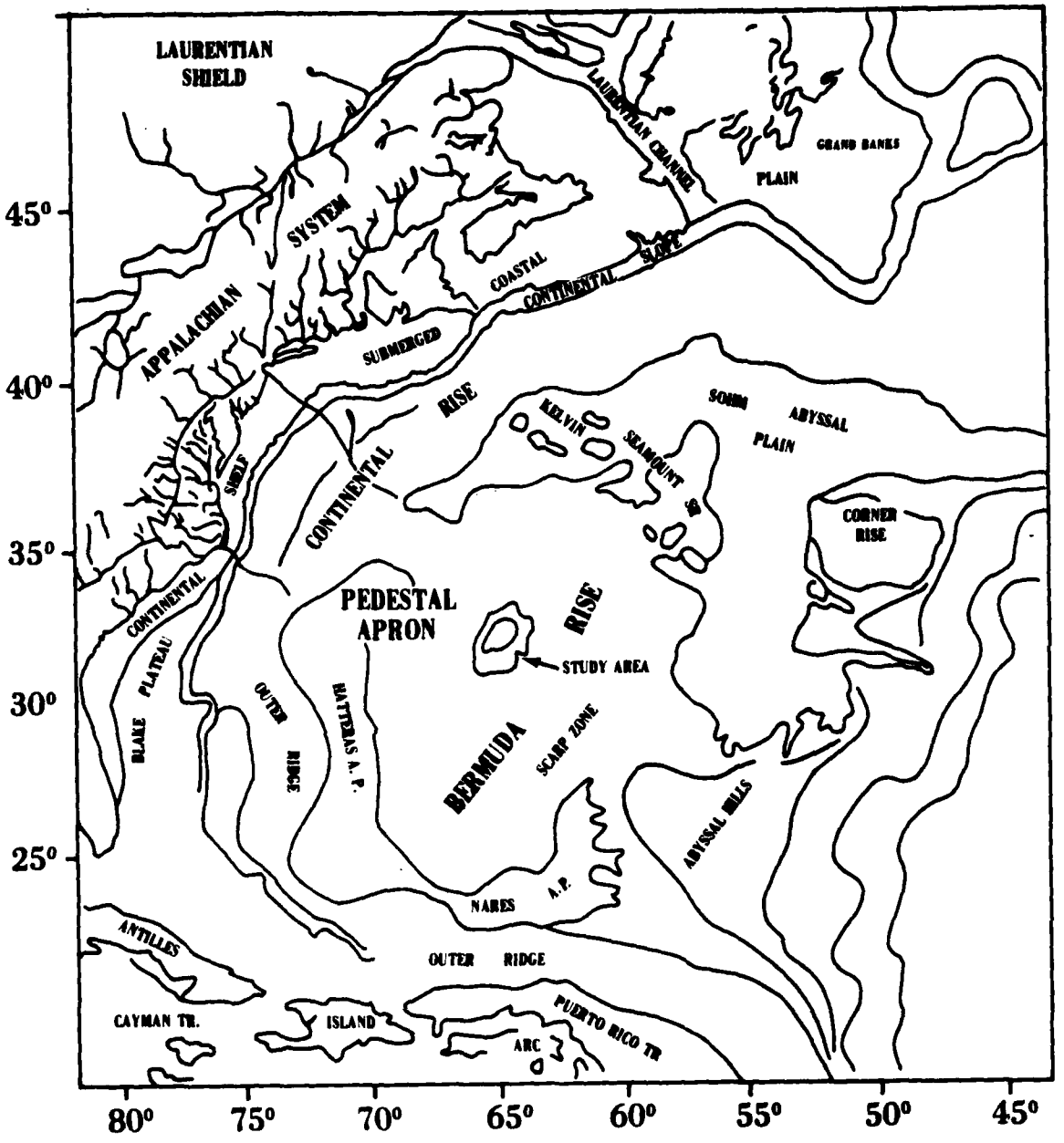

FIGURE 1. Physiographic province chart of the western North Atlantic showing location of this study (redrawn from Heezen et al., 1959).

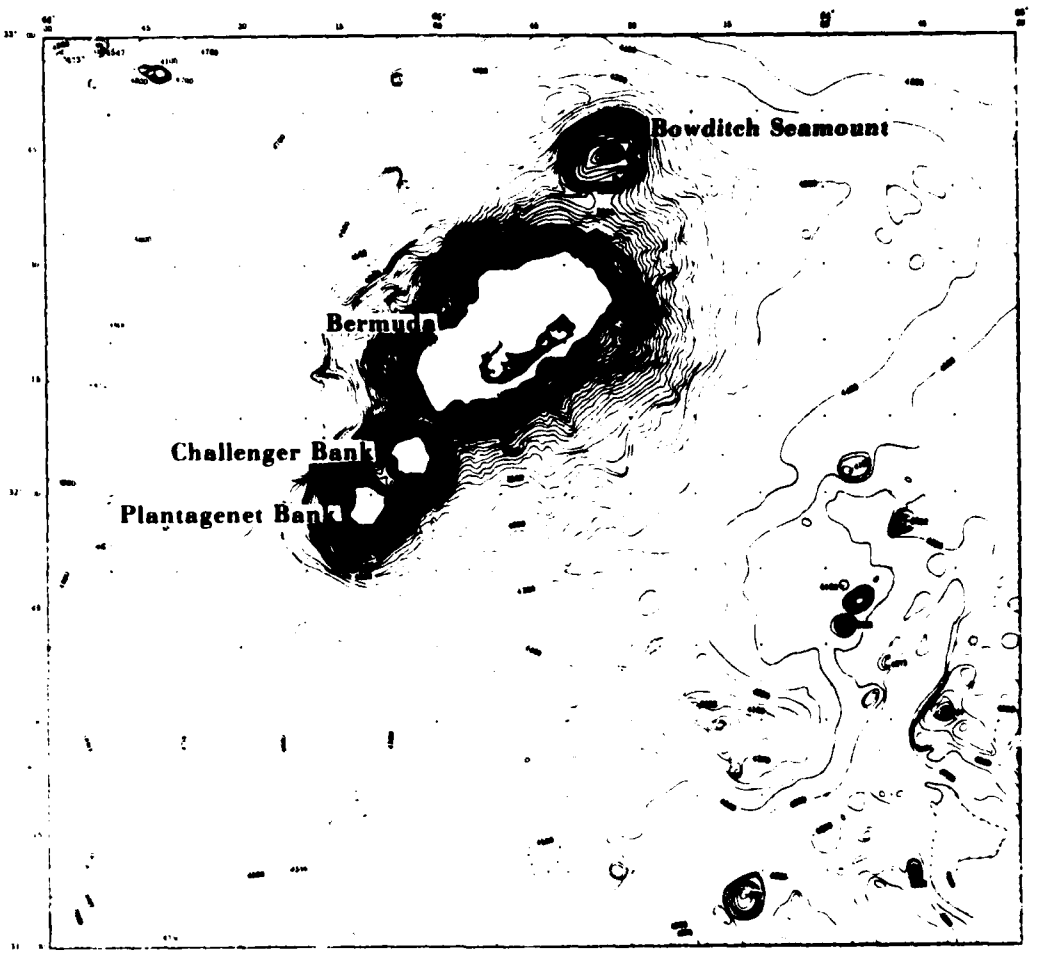

FIGURE 2. Bathymetry of the Bermuda Seamount.

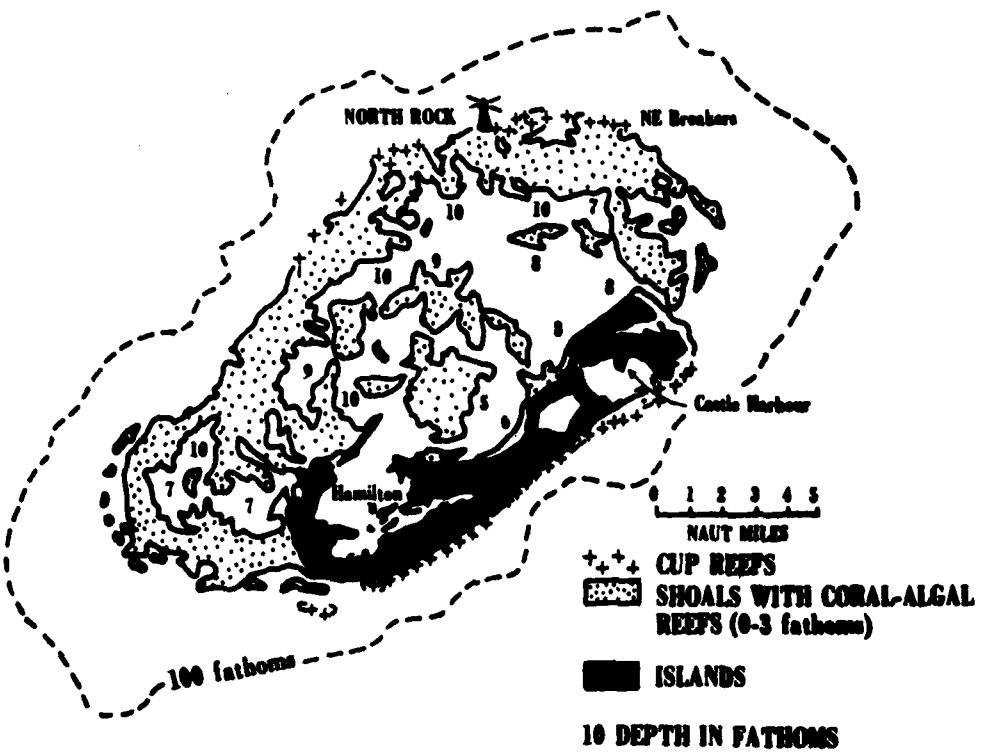

FIGURE 3. The Bermuda Platform showing the generalized distribution of reefs (redrawn from Ginsburg and Schroeder, 1973).

highs averages 20 to 55 km. The apron is considered to be an area of low relief, with elevations are between 18 and 95 m and gentle slopes (Figs. 1 and 2). The study area on the southeastern flank is an area of rugged topography, with relief of as much as 1004 m. The deepest portion of the study area is in 4725 m of water (Bowles, 1979, and Fig. 4).

Trending northeast to north-northeast along the axis of the Bermuda Rise are numerous fractures in the Cretaceous basement of the rise. The trace of this line of fractures is called the Bermuda Discontinuity (Vogt et al., 1971; Vogt and Ballard, 1976). The discontinuity separates rugged and fractured basement on the eastern side of the rise from smoother basement on the west (Fig. 1 and Bowles, 1979).

As early as 1907, Verill (quoted in Pirsson, 1914) suggested that the island of Bermuda formed during or at the end of Triassic times. Based upon data from a well drilled in an unsuccessful attempt to find water near Gibbs Hill, Bermuda, Pirsson (1914) proposed an Eocene or early Oligocene age for sediments found immediately overlying the volcanic rock and, hence, an Eocene or pre-Eocene age for the volcanic activity. Three subsequent drill holes in the Bermuda Islands penetrated igneous basement. The petrology and geochronology of core samples (Reynolds and Aumento, 1972) suggest two volcanic events occurred, separated by substantial time, to form the Bermuda Pedestal. The first consisted of tholeitte flows and was at least 60 to 80 million years before present (mybp) (potassium-argon dating), and perhaps as old as the time of the formation of the regional sea floor, 110 mybp (Vogt and Einwich, 1979). The Bermuda Rise and part of the Bermuda Pedestal could have been built at this time. By about 33 mybp the formation of the

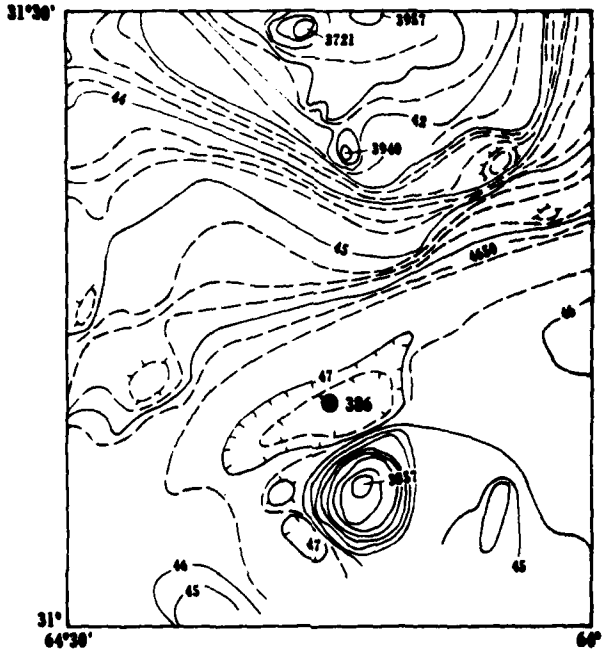

FIGURE 4. Bathymetric map of DSDP Site 386 contoured in uncorrected meters at 25 meter intervals. Solid circle indicates location of drilling site (from Bowles, 1979).

pedestal, or reactivation by intrusion of numerous steeply dipping (40° to 70°) lamprophyric dikes (Hyndman et al., 1974), was complete.

Physical Conditions

Currents

Sediments in the North American Basin of the Atlantic are strongly influenced by the Gulf Stream System to depths of about 4800 m (Fig. 5). The westward return flow of the system passes over and interacts with the northern flank of the Bermuda Rise. Associated with this return flow are a series of eddies that have significantly higher velocities than the main flow (30 cm/sec versus 19 cm/sec). These eddies are strong enough to resuspend bottom material, which the main flow then transports (Laine and Hollister, 1981).

Whereas ocean currents are generally most influential in depositional patterns over large areas of ocean floors, seamounts, guyots, ridges, etc., act as obstacles to circulating water masses carrying suspended sediment, and often localize deposional patterns by serving as collection foci for pelagic sediments (Stanley and Taylor, 1977). The Bermuda Seamount probably acts in this fashion. Currents around the seamount itself are not well understood. That they are substantial has been reported several times by Navy divers who have had to cancel submersible experiments because currents made diving risky (personal communication, James Matthews, NORDA). Unpublished Navy bottom photos on southern portions of the pedestal have revealed up to 50% exposed basalt, again evidence of strong current activity.

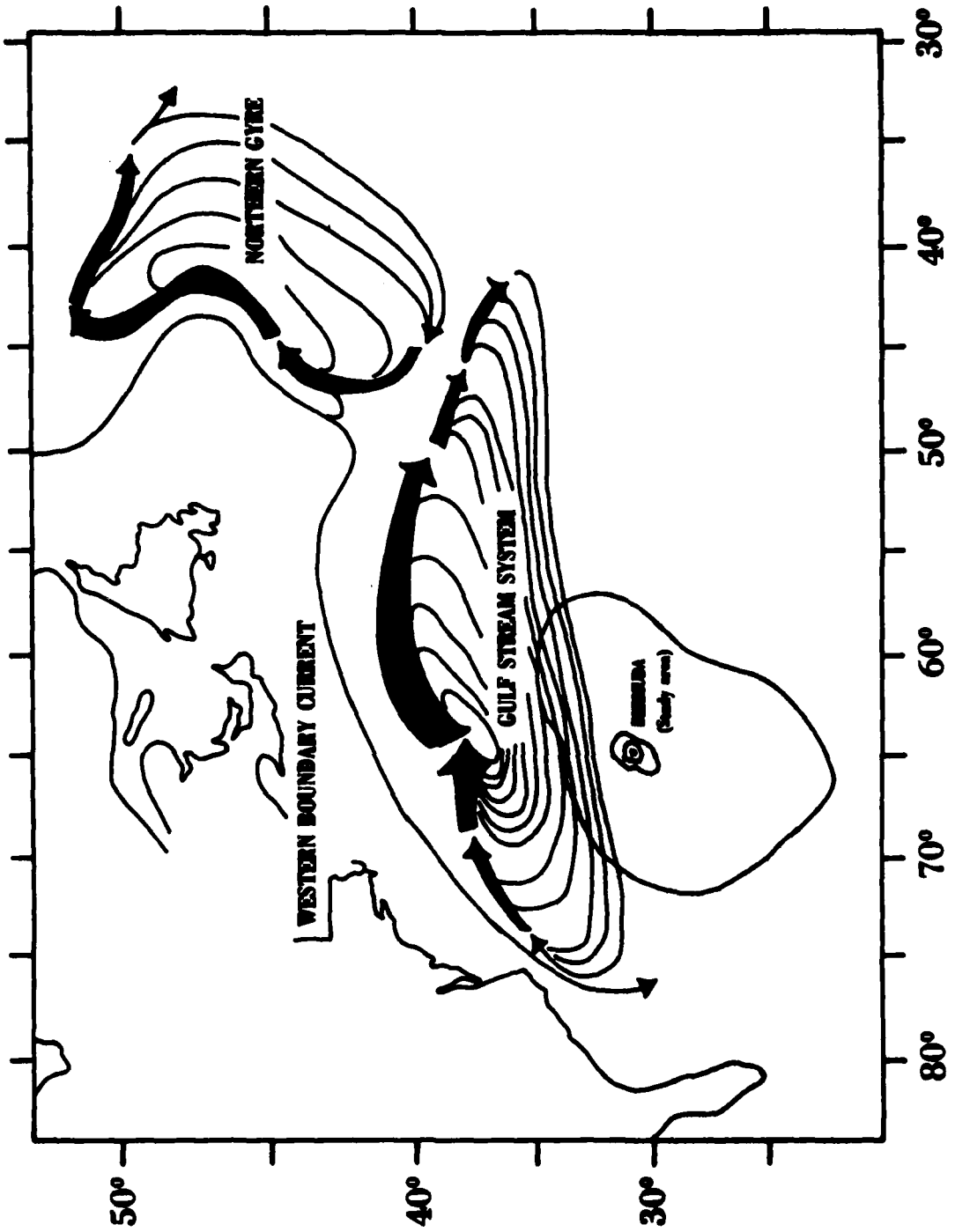

FIGURE 5. Location of the Gulf Stream System (from Laine, 1979). Study area extends in southeastern direction from Bermuda. Gulf Strea System intersects the northern portion of the Bermuda Rise above 4800 m.

In the northern Bermuda Rise, sediments consist of fine-grained hemipelagic lutites rich in illite. The ultimate source is presumably the east coast of Canada. During glacial portions of the Pleistocene, sediments were carried Southward from the St. Lawrence drainage basin by turbidity currents. As the transported material came in contact with bottom water of the Gulf Stream System, the finer fractions were entrained and were carried southward by the Western Boundary Undercurrent and to the east and west by the Gulf Stream System (Laine, 1979).

Below 4800 m, sediment is affected by North Atlantic bottom water rather than the Gulf Stream System. Deep water from the Norwegian Sea follows the eastern side of the Mid-Atlantic Ridge until it reaches the Charlie Gibbs fracture zone and passes through to the west side of the ridge. At this point, it joins deep water from the Labrador Sea to form a southerly current along the base of the continental margin below the Gulf-Stream System (Fig. 5).

The movement of water over the southern flank of the Bermuda Rise is not so well understood. Bowles (1980) shows evidence that long-term bottom currents to the southeast of Bermuda act in a southwest direction.

Deep water arriving from the Antarctic comes northward until it reaches the Mid-Atlantic Ridge (Fig. 6). Just southeast of Bermuda, this deep water splits, one portion continuing to the northeast, the other forming a counterclockwise current around the Bermuda Rise (Heezen and Hollister, 1971). Large cross beds, flutes, ripples, and scour marks on the rise attest to the strength of the circum-Bermuda current (Heezen and Hollister, 1971).

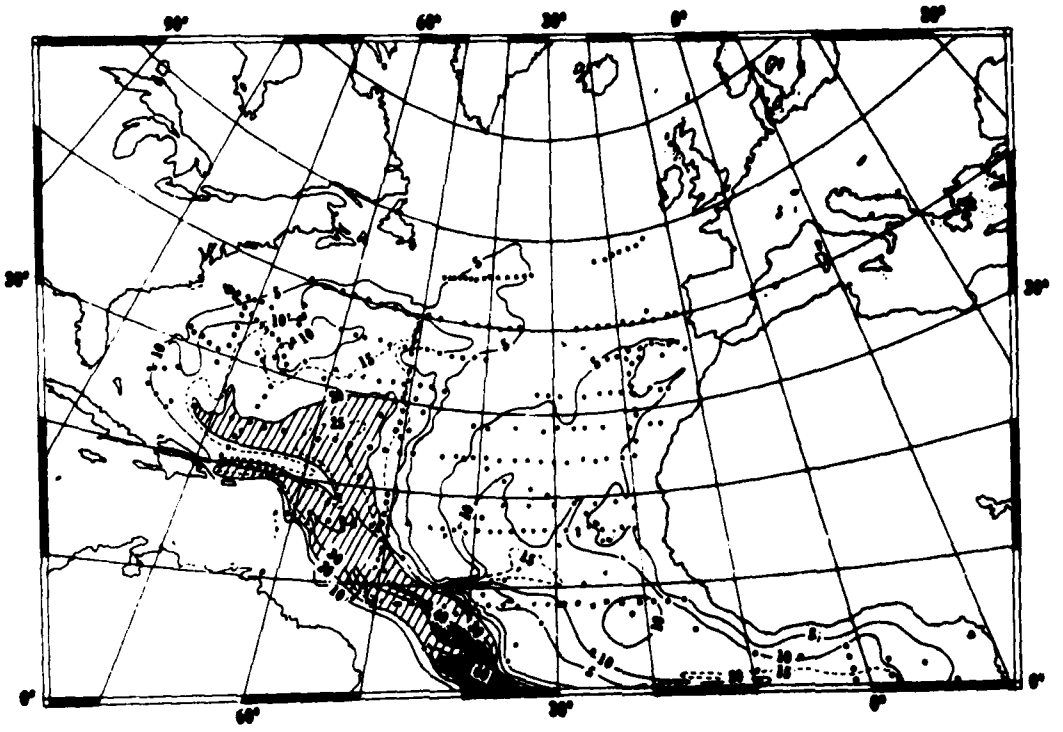

FIGURE 6. Distribution of Antarctic Bottom Water, contours in percent Antarctic Bottom Water (from Heezen and Hollister, 1971).

Winds and Climate

The winds on Bermuda blow primarily from the northwest during the winter months and from the southwest during the summer months. Wind speeds are fairly constant throughout the year, averaging between 5 and 15 knots (Naval Weather Service Command, 1974).

The entire area is influenced by the Bermuda High. During the winter months, November through March, several storms occur each month, but few are felt during the remainder of the year. Tropical storms average about one per year, with severe hurricanes averaging about one every 4 to 5 years. Tropical storm season is between May and November, with most storms during late August through October. Temperature extremes are between 6°C and 35°C, and the climate is largely controlled by the marine system (Naval Weather Service Command, 1974).

Waves

Since wave influence is negligible below 200 feet in this area, even the shallowest cores from which samples were analyzed were unaffected by wave action.

Temperature and Salinity

Bermuda (32°20'N, 64°45'W) is on the edge of reef building latitudes (between 30° north and south); temperatures are marginal most of the year for reef-building organisms (Stanley and Swift, 1968). Sea

surface temperatures vary between 18°C in March to over 27°C in August (Neumann, 1965). The shallow waters of the Bermuda Platform respond more markedly to atmospheric conditions, varying locally from 17° or less to over 30° in the summers.

Open ocean salinities vary little from 36.5% most of the year but decrease to near 16.0% during the rainy months from August to October (Neumann, 1965).

STRATIGRAPHY

Lithostratigraphy

Several DSDP holes have been drilled on the Bermuda Rise; Site #386 (31°11.21'N, 64°14.94'W) is the closest to the Bermuda Pedestal (Fig. 4). The lithologic section above basalt is dominated by typical ocean clays (illite and montmorillonite) and biogenic carbonate and silica (Fig. 7). At this site, the oldest deposit is a 240 m thick unit of greenish-grey and dark-grey and black claystone, which accumulated at the rate of about 16 m/my (DSDP, 1979). Inasmuch as the unit is less than one-third biogenic and the rate of deposition is an order of magnitude larger than the rate of skeletal production (DSDP, 1979), there must also have been an introduction of material by means other than pelagic settling of skeletal parts.

Above these claystones are zeolites and red claystones (Fig. 7). If zeolites represent altered volcanic ash, they may be indicative of an early phase of vulcanism on Bermuda.

The sequence of radiolarian mudstone, cherty claystone and calcareous turbidites (Fig. 7) was deposited at uniformly high rates of 20 to 40 m/my; many contain shallow water organisms (DSDP, 1979).

A single interval approximately 150 cm thick, representing middle Eocene to lower Oligocene, is composed of volcaniclastic turbidites (Fig. 7). During this interval the present Bermuda Pedestal formed, ceased to be active and was truncated. This section is often regarded as proof of the second volcanic event, dating the formation of the present Bermuda Pedestal at 35 mybp.

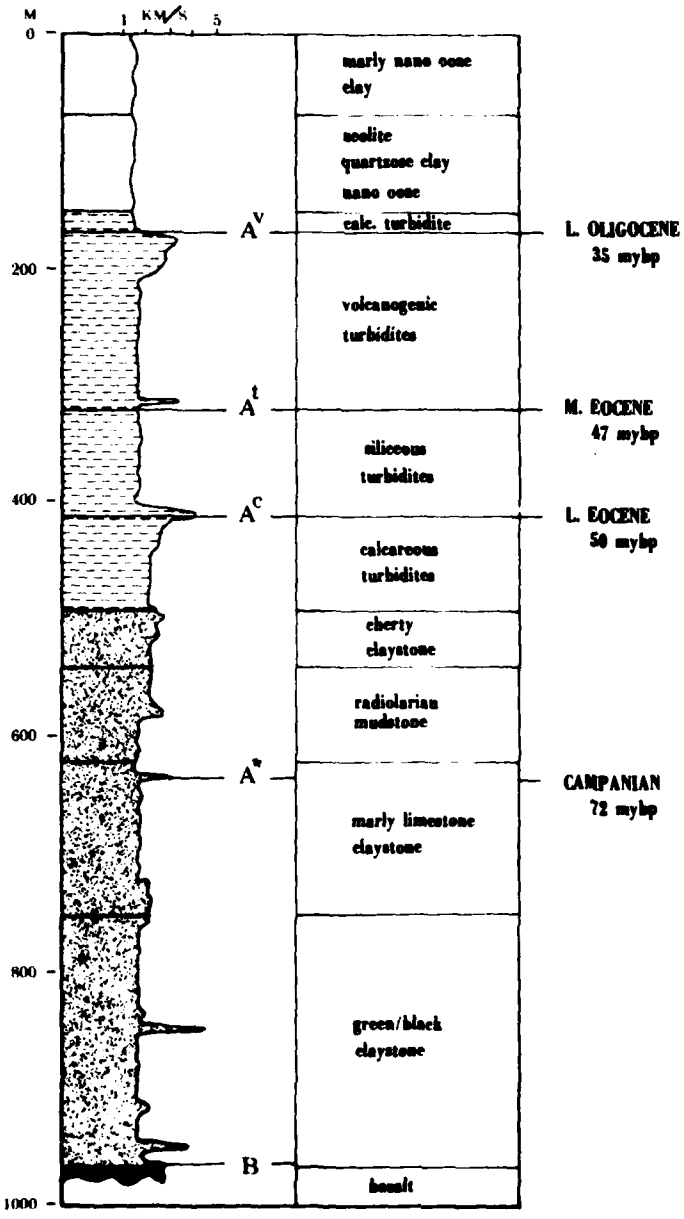

FIGURE 7. Stratigraphic section from DSDP Hole 386. A^V, A^t, A^C, and A* represent seismic reflectors comprising the North Atlantic Horizon A complex. Horizon B marks the top of seismic basement.

Above this section, the sediments are primarily pelagic carbonate oozes (Fig. 7) representing considerably lower rates of accumulation (about 6 m/my).

Seismic Stratigraphy

There are several prominent seismic-reflecting horizons in this region which are part of the North Atlantic Horizon "A Complex" (Tucholke, 1979). The stratigraphic section (Fig. 7) shows the correlation of these seismic horizons with cored lithology. Horizon A^v represents the top of the volcaniclastic turbidites (deposited approximately 35 mybp) and is commonly the strongest reflector in the Bermuda area. It becomes less prominent and disappears in either direction away from Bermuda. Presumably, this represents extensive erosion of the Bermuda Pedestal. The next two lower seismic horizons, A^t and A^c, are associated with Lower to Middle Eocene turbidites and are more widely distributed than Horizon A^v. Horizon A^t marks the top of turbidites with both biogenic and terrigenous components, which are not the result of local sediment redistribution. The most likely source of these sediments is the continental margin of North America (Tucholke, 1979). Horizon A^c corresponds to the top of cherts and may represent a diagenetic interface that is equivalent to Horizon A (Tucholke, 1979). Horizon B marks seismic basement and is generally felt to represent either the upper surface of basalt or of limestones "ponded" above the basalt.

The available seismic reflection profiles in the immediate vicinity of the Bermuda Pedestal (Fig. 8 and Appendix 5) show only Horizons A^v

FIGURE 8. Location of tracks for seismic profilesin Appendix 5. The stippled area represents sediment cover. Sediment cover is determined by plotting points where horizon A^v sediments pinch out (from seismic tracks, Appendix 3).

and sometimes B clearly. In all cases, Horizon B exhibits the irregular appearance of oceanic basalt. Between Horizon B and Horizon A^V, sediments appear stratified (Appendix 5) as would be expected from the deposition of volcaniclastic turbidites. Horizon A^V is concave upward between highs in Horizon B. This may be the result of compaction and settling both of the pre-A^V and Horizon A^V sediments. As the Bermuda Pedestal is approached, Horizon A^V increases in reflectivity, commonly masking the lower reflectors, including Horizon B. Some profiles, however, do show Horizons A^V and B converging to form a single reflector, which appears to become the sea floor reflector as the interval between the surface and Horizon A^V pinches out. The overall appearance is one of Horizon B rising to form the Bermuda Pedestal, with Horizon A^V onlapping it (Appendix 5). At the point where the water-sediment interface begins to shoal, the post-Horizon A^V sediments pinch out, leaving an acoustically opaque pedestal (Fig. 8). Above this point, neither seismic reflection nor 3.5 kHz profiles show detectable sediment accumulation.

METHODS

Samples were obtained from eleven cores stored in the core repository at Lamont-Doherty Geological Observatory. The cores were sampled at 10 cm intervals, starting with the very top interval, to a depth of 40 cm. The cores were taken in water depths ranging from 366 m to 4330 m (Table 1, Fig. 9). Results of ten additional cores analyzed by NAVOCEANO were also obtained (Table 2).

Samples were analyzed for (1) total carbonate content, (2) mineralogy by X-ray diffraction, (3) grain size by Elzone counter, and (4) identification of constitutent particles by scanning electron microscope examination.

Carbonate Analysis

Carbonate analyses were done using a manometric system according to the method developed by Hulseman (1966). All samples were ground with mortar and pestle and homogenized by shaking. They were then dried in a low temperature (250° F) oven overnight and stored in a desiccator jar until weighing. Between 0.15 and 0.3 g, depending on the carbonate content of the sediment, were weighed on an analytical balance for each analysis. This small sample was then added carefully to a pyrex container. The leveling tube of the Hulseman apparatus was then raised until the burette read 0. The system was closed with a 3-way stopcock. Three milliliters (ml) of 4N HCl were added. When the reaction ceased, the sample was heated with a Bunsen burner until a rolling boil was

TABLE 1. LOCATION OF PEDESTAL AND APRON CORES (FROM HERE ON SIMPLY CALLED PEDESTAL CORES) AND WATER DEPTHS FROM WHICH THEY WERE TAKEN

Core Id	Location		Depth (m)
V5-5	32°15.8'	64°44'	366
C10-10	32°19'	64°34'	1002
C22-5	32°17'	64°38'	1094
C10-7	32°20'	64°34'	1147
V5-8	32°10.20'	64°30.59'	1150
C22-6	32°16'	64°35'	1505
C22-2	32°11'	64°45'	1939
C10-11	32°14'	64°32'	2026
A164-25	32°13'	64°31'	2945
V7-65	32°07'	64°47'	2970
V19-3	32°11'	64°10'	4330

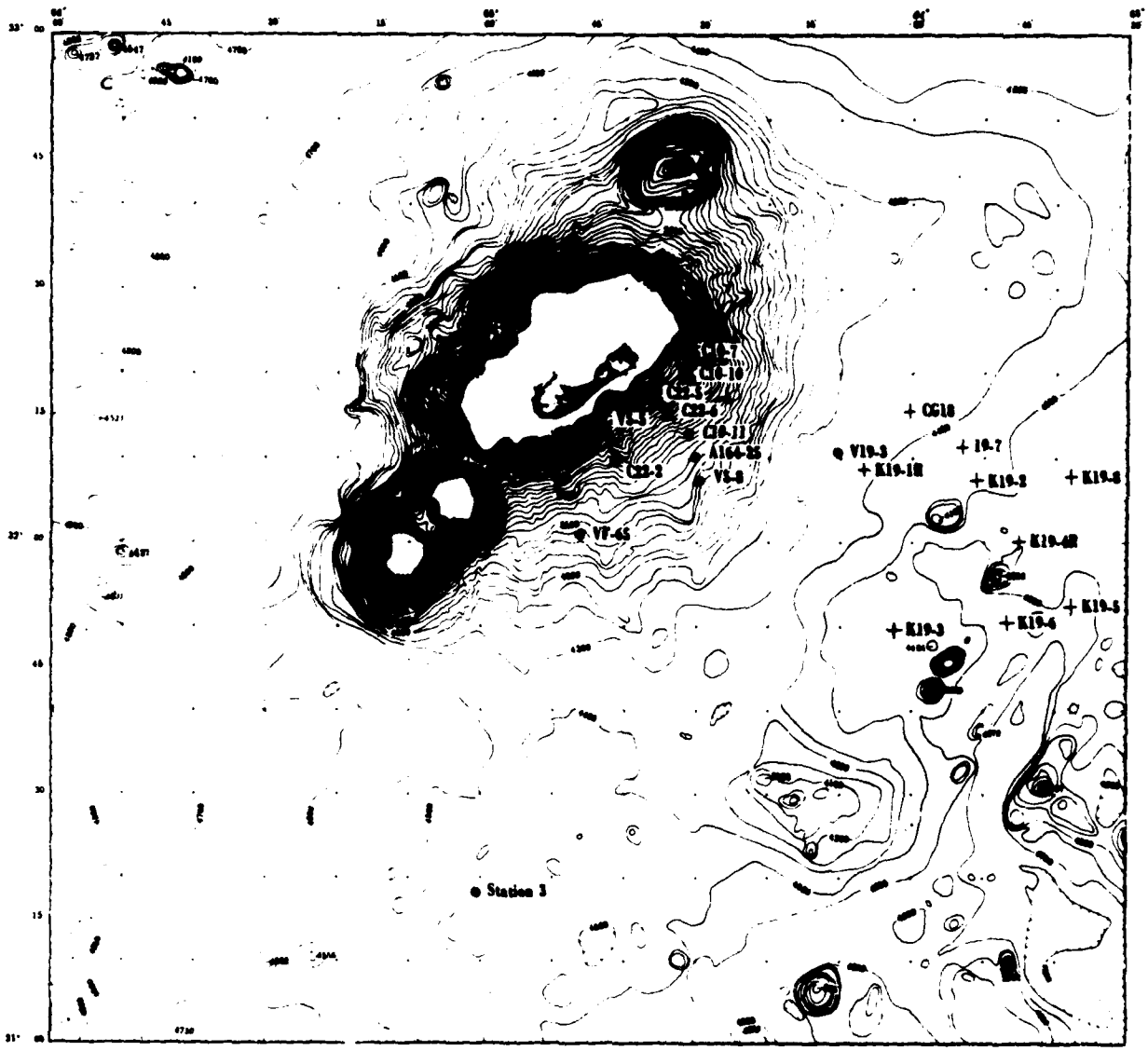

FIGURE 9. Location of cores.

+ = pedestal and apron cores samples for this study

● = rise cores (NAVOCEANO)

TABLE 2. LOCATION OF RISE CORES (NAVOCEANO) AND WATER DEPTHS FROM WHICH THEY WERE TAKEN

Core Id	Location		Depth (m)
K 19-1R	32°8.50'	64°7.20'	4365
CG-18	32°14.8'	64°0'	4382
19-7	32°11.7'	63°55.2'	4410
K19-3	31°49.4'	64°2.6'	4490
K19-4R	32°00.10'	63°45.5'	4520
K19-8	32°6.8'	63°38'	4555
K19-5	31°52.3'	63°53.9'	4620
K19-2	32°6.0'	63°53.9	4425
K19-6	31°51.1'	63°46.3'	4620
Sta 3	31°17.0'	64°58.5'	4450

achieved. The sample was then quickly cooled with cold water and allowed to equilibrate 14 minutes.

The mercury in the leveling bulb was adjusted so that it was level with the mercury in the burette. The volume of carbon dioxide (CO_2) was read directly from the burette. The amount of CO_2 generated was then determined manometrically using the following formula (Hulseman, 1966) based on the gas laws (PV=RT).

$$CaCO_3 + 2HCl \quad CaCl_2 + H_2O + CO_2$$

The formula for computing the amount of carbonate can be written:

$$\%CaCO_3 = \frac{V(P-M)}{W(T+t)} \times 0.163 \qquad \text{(Weast, 1964, p 192)}$$

V=observed volume of CO_2 in ml (read from the burette)

P=barometric pressure in mm Hg

M=vapor pressure of water in mm Hg, dependent on the lowest temperature in the system (usually the temperature of the cooling system, Appendix 3)

W=weight of the sample in g

T=room temperature in degrees C; in order to compensate for variations between the beginning and the end of the analysis the average of the two temperatures is entered

t=degrees Kelvin (273.2 added to degrees C)

0.1603 is a constant resulting from the conversion of the barometric pressure to CGS units and the molecular weight of $CaCO_3$.

The accuracy of the method was checked periodically throughout the day by analyzing a known amount of calcium carbonate (Allied Chemical, Reagent Grade ACS code 1506). The system was considered to be accurate if standards fell with $\pm$ 2% of the correct value. It was assumed that samples also fell within the same range.

The 14 minute thermal equilibration time was determined experimentally for this system with $CaCO_3$ standards.

X-Ray Analysis

Samples were separated into 3 size fractions by a combination of settling and seiving techniques. All samples were first placed in a 500 ml flask with 15 ml 0.1 N Calgon solution (dispersant). The volume was then brought to 300 ml with distilled water (5 cm in depth) and shaken thoroughly. Three hours 32 minutes later, assuming a settling distance of 5 cm, the supernatent was siphoned off. Time was calculated using this formula from Folk (1974):

$$T \text{ min} = \frac{\text{depth in cm}}{1500\ (A)\ (d)^2}$$

$$212 \text{ min} = \frac{5\text{cm}}{1500\ (343)(.002)^2}$$

A=density at a specific temperature

d=diameter of the particle

This was repeated 3 to 4 times until the supernatent was clear. The supernatent was assumed to contain the clay-size fraction (less than 2 m); the remainder equaled the silt plus sand-size fractions.

The sand and silt fractions were separated by wet seiving using a #230 (63μm) seive.

These size fractions were then dried and powered. All were X-rayed on a General Electric Diffractometer, XRD 5, as powder mounts at 1°/2θ, 30 mA and 45 KV. A silica standard was then added to each sample, which was then rerun using the same settings.

Amounts of low and high-magnesian calcite were calculated according to Milliman (1974, p 23, Fig. 10). The area under the peaks was calculat calculated using a planimeter. The area under the free half of the major peak, the right side of the low-magnesian calcite peak, was calculated and multiplied by 2. This area was then compared to the total area in order to differentiate between it and the other calcite peaks present. The percentage of magnesian-calcite was then calculated according to the formula given by Milliman (1974, p 23, Fig. 10).

The aragonite percentage was similarly calculated using the area under the 26.24 Å peak and comparing that value to a standard curve published in Milliman (1974, p 24, Fig. 11).

An attempt was made to derive a standard curve for the Bermuda area using organisms from these particular samples. Pteropods were used as the aragonite source and planktonic forams as the low magnesian calcite source. However, the very small size of tests made the separating process difficult. Most of the pteropod tests were filled with much smaller tests, generally of pelagic forams, thus it was impossible to obtain a pure aragonite sample.

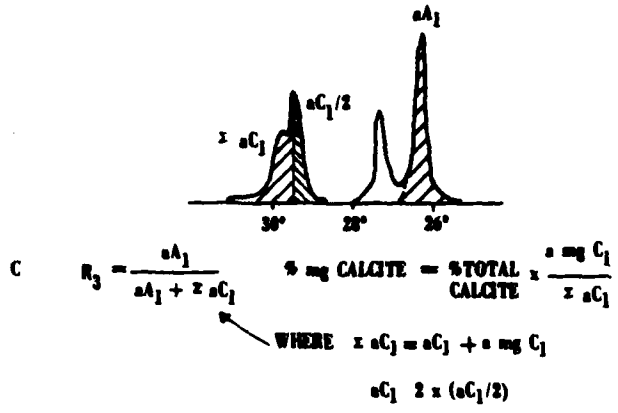

FIGURE 10. Method for calculating percent magnesian calcite (Milliman, 1974, p. 23).

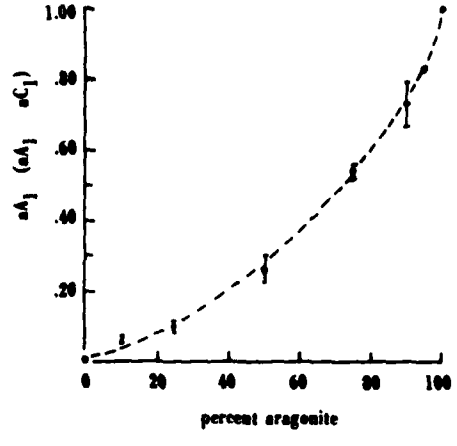

FIGURE 11. Standard curve for aragonite determination using peak area analysis. Each data point represents 8 to 10 analyses of various calcite and aragonite (Milliman, 1974, p. 24).

Scanning Electron Microscopy

The sand size fraction of each sample was dried and randomly fixed to sticky tape on an SEM stub by dipping the stub in the sand-sized fraction and turning it until an even coating was achieved. The clay-sized fraction was diluted with distilled water and filtered onto a 0.4 m Nuclepore filter (Nuclepore Corp., Pleasanton, Ca.). This was then dried and attached to an SEM stub with double-sided tape. Samples were then edged with silver paint to reduce charging. After thoroughly drying, the samples were coated with a thin film of gold using a Polaron E5100 Sputter Coater (Polaron Equipment, Ltd., Dolyesville, Pa.)

Samples were examined with a scanning electron microscope AMR Model 1000 (Advanced Metal Research, Inc., Bedford, Ma). Five fields were selected at random and photographed at 50X on each stub of sand-sized fraction so that organisms could be identified. A 3/4" by 3/4" grid was utilized to aid in counting. Generally all organisms in a field were counted. Occasionally when the organism density was too great to count, every other square was counted.

Huang and Pierce (1971) have pointed out the difficulties of determining sources of carbonate grains and sediments in fine sands and silts. Therefore, only the sand fraction was examined for the purpose of estimating relative abundances of constituent particles. The clay size fractions were scanned only to determine qualitatively the primary constituents. No attempt was made to count organisms.

Grain Size Analyses

The amount of material available for grain size analysis was approximately one gram, which necessitated the use of electronic techniques rather than the traditional pipette or settling tube methods. The instrument used was an Elzone 80XY (Particle Data, Inc., Elmhurst, Ill.). The basic detection principle of this instrument is the same used in the Coulter Counter, i.e., a particle suspended in an electrolytic medium passes through a micro-orifice, displacing an amount of electrolyte equal to its volume, thus causing a change in an electric field applied across the orifice which is proportional to the volume of electrolyte displaced. The Elzone differs from the Coulter counter primarily in how this electronic pulse is processed, and it produces a more rapid analysis and a finer resolution of the size versus frequency distribution.

The property measured by the Elzone technique is particle volume; the data actually read from the instrument is the diameter of a sphere having the equivalent volume, the conversion being done automatically. This is not the same property measured by the pipette method which is based on the Stokes relationships and mass. However, for particle systems such as the core samples analyzed for this work, in which the densities are fairly uniform and in which the dominant shape is sub-spherical, the two techniques should give comparable results, as was found by Kelley (1981) in a comparison of size distributions of suspended sediment.

Sample preparation was as follows; 50 to 100 mg of sediment was dispersed for a minimum of 10 minutes in an ultrasonic bath in 3 ml of a dispersant/electrolyte solution consisting of 10 g/l calgon (commercial sodium hexametaphosphate dispersant) and either 19 gm/l or 100 gm/l anhydrous sodium sulfate. Preliminary examination indicated that there were few statistically significant particles over 150μm equivalent diameter, so the upper size limit for the analysis was chosen to be 210 m. The lower limit of detection for the instrument used is 0.7 m. Thus the size range considered was approximately 10.5 ϕ to >2.0 ϕ.

In order to prevent blockage of the orifices by particles larger than the orifice diameter, the sample was sequentially screened through 210μm, 70μm, and 10μm, nylon mesh (Spectrum Medical Industries, Los Angeles, Calif.) using a 10 ml syringe as a funnel and a 25 mm-diameter in-line filter holder (*Nuclepore Corp.*, Pleasanton, Calif.) for the nylon mesh. This resulted in approximately 5 ml of suspension for each fraction (i.e., <210μm, <70μm, and <10μm). Each screening was done on a thoroughly mixed suspension and was followed by a rinse of 7 ml dispersant/electrolyte in order to maintain the original relative proportions in the size distribution, an important prerequisite for the data blending steps to come later. For the analysis, each suspension was thoroughly mixed and diluted with filtered dispersant/electrolyte to yield a coincident count rate of 1% or less (i.e., 1% or fewer of the counts are the result of two or more particles passing through the orifice at the same time).

Each size fraction was analyzed using a different sized orifice because the analytical range for any given orifice is from 2 to 60% of

its diameter. The three distributions obtained overlapped considerably, allowing each distribution to be normalized to the smaller distribution adjoining it. The resulting "blend" is thus a properly proportioned size versus volume (or mass) distribution over the entire range of interest. The amount of material was integrated over 0.5 phi intervals and the percentages of clay, silt, and sand computed. Data were recorded digitally, processed, and graphed using an HP 9825B computer system (Hewlett-Packard Co., Palo Alto, Calif.).

Limitations of the Data

Sampling of cores used in this study was performed by Rusti Lotti, assistant to Dr. Floyd McCoy, Curator of Lamont-Doherty Geological Observatory Core Repository. This researcher was not able to inspect the cores. These cores were obtained between 1959 and 1974, and were stored in PVC core liners wrapped in plastic and refrigerated, which should allow preservation, in good condition, for years. In spite of this storage, moisture was lost from older cores. This probably did not affect the analyses that could be performed. Physical measurements such as sound velocity, water content, and specific gravity, could not be performed on cores of this age.

Between 1959 and 1974, both coring and navigation techniques improved considerably. The depth at which cores are recovered is measured either in terms of amount of wire line payed out, or with a fathometer. On slopes of 30° either technique may result in inconsistencies between depth recorded for cores and depth apparent when core locations are

plotted on a bathymetry map. Some depths also were recorded in corrected (for temperature, salinity, etc.) meters by Lamont-Doherty at the time of coring; others, in uncorrected meters (NORDA). Corrected core depths were converted to uncorrected meters by use of Matthews Tables (Bialek, 1966) inasmuch as the bathymetry was also compiled in uncorrected meters, a source of possible error.

Early navigation was based on celestial fixes; satellite navigation became available by the early 1970's. Thus, early core locations may be accurate only to within $\pm$ 10 km.

Two different methods were used to analyze samples for grain size and carbonate content. NAVOCEANO calculated grain sizes with a Micromeritics system, this researcher, with an Elzone Counter. Total carbonate content by NAVOCEANO utilized a carbonate bomb similar to that used by the DSDP (DSDP, 1978). This researcher used a manometric gasometric system (Hulseman, 1966). Several different technicians also performed the NAVOCEANO analyses. However, results of pedestal core analyses for this study can be considered consistent (done by the same method by the same person). Data from NAVOCEANO and DSDP Leg 43 were included primarily to enhance the picture formed from analyses of the 11 main cores from the pedestal.

RESULTS AND DISCUSSION

Morphology

By plotting the points where post-Horizon A^V sediments pinch out (Fig. 8), it becomes clear that the apparent "apron" (zone of 2.5° to 3.8° slopes) is seismically opaque with no detectable accumulation of soft sediment. At the base of the pedestal, therefore, there is no significant depositional apron produced by the downslope transport of post-Horizon A pelagic sediments. The apron is more likely a volcanic or volcaniclastic feature associated with Eocene-Oligocene volcanic activity when the Horizon A^V sediments were being deposited. The term "apron", therefore, probably should not be used because of the sedimentary connotation associated with the term. The slopes of the pedestal are sparsely covered with sediment. Unpublished Navy photos (J. Matthews, personal communication) reveal up to 50% exposed basalt in some areas. This pedestal and apron description is quite consistent with that of Cotton (1969) in terms of reported slope zones on Pacific and Indian Ocean seamounts and with his concept of a central core of basaltic flows surrounded by a talus slope of volcaniclastics.

There is evidence of down-slope transport of post-Horizon A^V sediments. Seismic line cross sections A-A', B-B', C-C', E-E' and F-F' (Appendix 5) show examples where the post-Horizon A^V sediments pinch out against the base of the pedestal. This region often shows an irregular water-sediment interface suggestive of slumps. Unpublished NAVOCEANO 3.5 kHz profile data in this area show irregular hyperbolae of the

Damuth (1980) type IIIC, but with evidence of subbottom layering. Higher on the pedestal than the point of apparent post-Horizon A^V pinchout, no subbottom layering is detectable. Profiles B-B', D-D' and E-E' (Appendix 5) also show what are interpreted to be shallow ponds of pleistocene deposits (Bowles, 1981). The volume of materials in these slope base deposits is not great, which is consistent with the relatively low post horizon A^V depositional rates (6 m/my) for sediments cored at DSDP Site #386.

Carbonate Content

The results of the carbonate analyses for the pedestal cores are listed in Table 3 which also shows the carbonate data for the tops of the ten rise cores analyzed by NAVOCEANO. As expected, the percentage of carbonate is generally high, averaging 87% overall, with 76% of the 43 samples composed of at least 80% carbonate and 33% of these cores composed of at least 95% carbonate.

Variations in carbonate content within the upper 40 cm of the cores range from virtually none (within the $\pm$ 2% precision of the system) to considerable. The extreme values are found within the 20- and 30-cm intervals of cores C22-5 and V7-65. These two cores also differ in color; instead of the usual creamy white, they are mustard yellow. They have a high content of clay minerals (see mineralogy section) of 72% and 60% in C22-5 and 45% and 43% in V7-65 (Table 3, Appendix 6). The amount of variability within the cores does not seem to be related to their location.

TABLE 3. TOTAL CARBONATE CONTENT FOR BOTH PEDESTAL AND RISE CORES

TOTAL CARBONATE CONTENT

Pedestal Cores

Core	Top %	10 cm %	20 m %	30 cm %	Avg %
C22-6	83.36	96.54	90.21	90.90	90.25
C10-10	96.82	95.53	94.06	93.10	94.88
C10-11	65.73	77.94	79.22	77.07	74.99
C10-7	93.50	95.00	90.92	93.10	93.13
C22-5	98.17	98.77	27.99	39.09	66.01
C22-2	95.21	92.83	90.10	93.18	92.83
V5-8	91.63	93.78	93.18	93.32	92.98
V7-65	86.28	89.83	54.64	56.86	71.90
V19-3	75.86	92.90	85.87	93.16	86.95
V5-5	-	96.06	98.83	97.91	97.60
A164.25	95.80	97.22	97.22	98.10	97.09
					87.15

NAVOCEANO TOPS

Rise Cores

K19-6	97
K19-2	59
K19-5	28
K19-8	61
K19-4R	84
K19-3	24
K19-7	53
GC-18	-
K19-1R	96
Sta 3	21.5

Clay Mineral Content

	20 cm	30 cm
C22-5	72	30
V7-65	45	43

In shallow water, the rate of supply of calcareous tests to the system generally exceeds the rate of dissolution; thus carbonate sediment accumulates. As calcareous tests are deposited in ever deeper water, the rate of dissolution begins to increase until such a depth is reached where the rate of dissolution equals the rate of supply. At depths below this zone, the carbonate compensation depth, the rate of dissolution is large enough that carbonate sediment does not accumulate (Johnson et al., 1977). Thus one would expect that, all other variables held constant, total carbonate content should decrease with increasing depth of water.

In a plot of total carbonate content versus depth (Fig. 12), there is a general trend of decreasing carbonate content with increasing depth. The general trend is similar between the various intervals of the cores (Fig. 12). Correlation coefficients (R) for the top-cm 10-cm 20-cm, and 30-cm intervals respectively are -0.453, -0.247, -0.062, and -0.011 indicating that the top intervals of the cores show more correlation between carbonate content and increasing water depth than does each lower interval in the cores.

The shallowest core, V5-5 (366 m), has an average (over all intervals within the core) carbonate content of 97.6% in the top 40 cm. Within the limits of the Hulseman system, this can be considered a totally carbonate sediment. The deepest pedestal core, V19-3 (4330 m) near the carbonate compensation depth (CCD) of 4400 to 4500 m in this area (Bowles, 1980), has an average carbonate content of 86.90%, only 10% less carbonate content than the shallowest core. When the average carbonate content of the cores is plotted against increasing water depth,

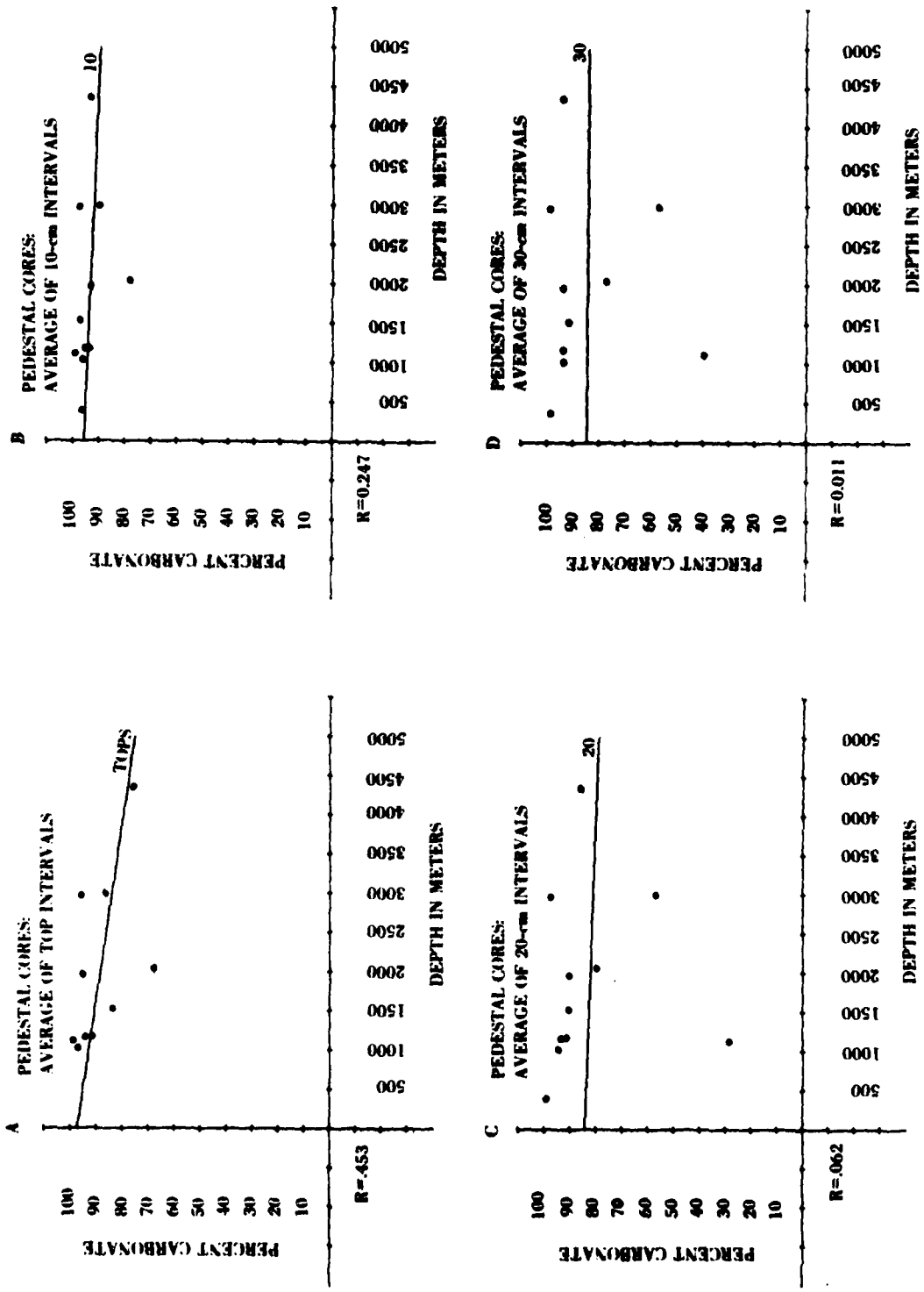

FIGURE 12. Total carbonate content of various intervals of pedestal cores.

the correlation coefficient is very weak (-0.188). When the carbonate content of the top intervals of the apron cores are plotted with the carbonate values for the pedestal cores, the correlation coefficient is -0.571, indicating that there is a reasonable strong correlation between increasing water depth and carbonate content (Fig. 13). As is evident, there is a good deal of scatter in the data.

Two possible reasons account for the decreasing carbonate content of sediments with increasing water depth: (1) dissolution of carbonate particles and (2) greater clay deposition as lower portions of the pedestal are reached. In a study of the effects of dissolution in carbonate sediments on the Ontong Java Plateau, Johnson et al. (1977) discovered calcium-carbonate content decreases with increasing water depth from 80% to 90% at their shallowest depths (1600 m) to less than 75% at their deepest (4500 m). The CCD there is around 5000 m. They concluded that this change in composition represented a loss of calcium carbonate to dissolution, which they calculated with the following formula:

$$L = (1 - Ro/R)\ 100$$

where

L = $CaCO_3$ lost in % of total sediment, to increase the insoluble fraction Ro, to R%.

R = weight % of noncalcareous material in the sediment sample from which L is calculated.

Ro= weight % of noncalcareous material in a sediment which has undergone no dissolution.

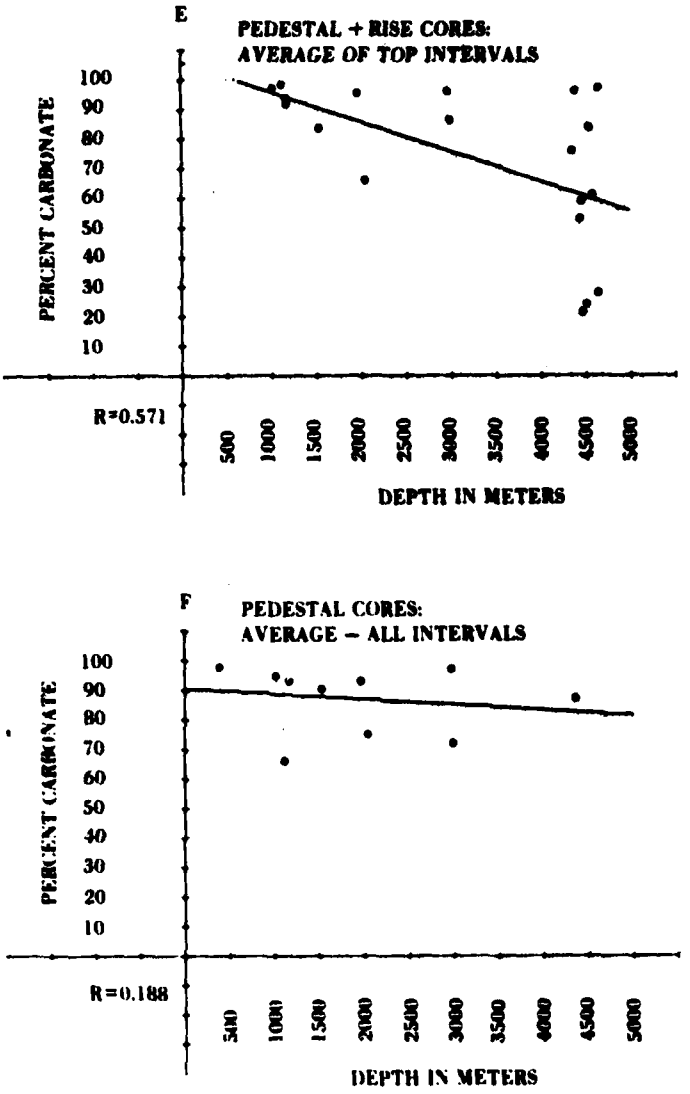

FIGURE 13. Carbonate content vs. water depth.

If it is assumed that sediment with the highest percentage of calcium carbonate has undergone no dissolution (V5-5 with average carbonate value of 97.6%), then L can be calculated setting Ro to 2.4%. Such calculations suggest, for instance, that up to 91% carbonate has been removed from V7-65 and 81.6% from V19-3, two of the deeper burial sites (Table 4). Johnson et al. (1977) suggest, however, that other factors probably affect calcium percentages, and they consider it unlikely that estimated values above 3000 m chiefly reflect dissolution. Similarly, the scatter in the data and the variation in depths of burial (Figs. 12 and 13) suggest that dissolution is only a part of the picture.

Increasing deposition of clay minerals on the lower pedestal may dilute the total percentage of carbonate sediment in the samples. As stated earlier currents may actively resuspend and redeposit sediments on the rise and possibly the lower reaches of the pedestal. The Pleistocene rocks of Bermuda consist of shallow water, beach, and intertidal marine biocalcarenites, eolianites, and red soils (Land and Mackenzie, 1970). Erosion of red soils from the platform may be contributing small amounts of clay minerals to the lower slopes of the pedestal.

Bathurst (1971) suggests a number of variables that weaken the correlation between calcium carbonate content of sediments and water depth, such as coating of particles with organic compounds and distance from land. It is difficult to access the amount and effect of particle coating without resampling specifically for that purpose. However, Land and Mackenzie (1970) state that the Harrington Formation on Bermuda was

TABLE 4. PERCENT CARBONATE LOST TO DISSOLUTION

CARBONATE DISSOLUTION

$L = 1-Ro/R$

V5-5	0%
A164-25	15.96%
V19-3	81.61%
V7-65	91.46%
V5-8	65.81%
C22-2	66.53%
C22-5	92.94%
C10-7	65.07%
C10-11	90.40%
C10-10	53.13%
C22-6	75.38%

deposited during the Harrington Regression when sedimentation rates were slow and large amounts of organic humus were present. The humus produced a "waxy" coating around each grain, thus preventing alteration, at least on the platform. Such "waxed" particles may be slower to undergo dissolution than uncoated particles. One can speculate about the effect of the proximity of the core sites to Bermuda. All are directly downslope from exposed land (possible source of noncarbonate sediment) and within 40 miles of the islands. Slopes range from 30° to 13° to 2.8° on the pedestal (Fig. 2).

It is reasonable to suppose that with slopes of this magnitude slumping is a definite possibility. At the same time, turbidity flows may be generated and, indeed, there is evidence of turbidite deposition in seismic profiles E-E' (Appendix 5). Such rapid transport would reduce time available for dissolution, thus preserving by burial larger amounts of carbonate in some areas than one would expect.

Bulk-Sample Carbonate Mineralogy and Skeletal Constituents

The carbonate minerals in the pedestal cores are primarily aragonite, calcite and magnesian calcite (Table 5). Two of the cores, C22-5 and V7-65 contain the clay minerals kaolinite, illite, palygorskite, and montmorillonite at the 20- and 30-cm intervals (these are the two cores low in total carbonate at those intervals). The other core samples were not x-rayed because after removal of carbonate there was not sufficient material remaining sample.

The pedestal cores can be arranged in three major groups: (1) those containing only calcite, (2) those containing calcite and aragonite, and (3) those containing calcite, aragonite and magnesian calcite.

1. *Cores containing only calcite:*

Three cores, C10-10, C10-11, and A164-25 fall in this category. The mineralogy of these cores correlates well with their constituent particles (identified by scanning electron microscopy; Table 6) which consisted of about 99% planktonic forams; these were identified mainly by shape (Fig. 14). Interestingly, grains in both C10-10 and A164-25 are well micritized.

2. Cores containing calcite and aragonite:

X-ray diffraction patterns of V19-3, V7-65, V5-8, and V5-5 reveal only calcite and aragonite in the sand- and silt-size fractions. In the clay-size fractions, V5-8 contains magnesian calcite (35%) as well as calcite (48%) and aragonite (17%). V19-3 contains possibly a small

TABLE 5. CARBONATE MINERALOGY OF THE SAND, SILT AND CLAY FRACTIONS OF THE PEDESTAL CORES

	Mineralogy		
Sand Fraction	Aragonite	Calcite	Mg Calcite
V5-5	26	74	-
C10-10	-	100	-
C22-5	41	28	31
V5-8	47	53	-
C10-7	40	13	47
C22-6	39	28	33
C22-2	26	36	38
C10-11	-	100	-
A164-25	-	100	-
V7-65	11	89	-
V19-3	36	64	-
Silt			
V5-5	39	61	-
C10-10	-	100	-
C22-5	35	13	52
V5-8	50	50	-
C10-7	28	23	49
C22-6	34	23	44
C22-2	36	24	40
C10-11	-	100	-
A164-25	-	100	-
V7-65	10	90	-
V19-3	19	81	poss a sm amt,
Clay			
V5-5	38	67	-
C10-10	-	100	-
C22-5	28	48	24
V5-8	17	48	35
C10-7	24	27	49
C22-6	26	57	17
C22-2	19	47	34
C10-11	-	100	-
A164-25	-	100	-
C7-65	3	97	-
V19-3	8	92	-

TABLE 6. CORRELATION BETWEEN SKELETAL COMPONENTS AND MINERALOGY

SKELETAL COMPONENTS*

Core	Skel components	Mineralogy
V5-5	M - PF - ES - SS	A - Ca
C10-10	PF	Ca
C22-5	PF - M	A - Ca - MgCa
V5-8	PF - C/A - M	A - Ca poss MgCa
C10-7	PF - M - SS - ES	A - Ca - MgCa
C22-6	PF - M	A - Ca - MgCa
C22-2	PF - M	A - Ca - MgCa
C10-11	PF	Ca
A164	PF	Ca
V7-65	PF - M	A - Ca
V19-3	PF - C/A	A - Ca

*M: Molluscs
PF: Planktonic Foramenifera
ES: Eschinoid fragments
SS: Sponge spicules
C/A: Coral and Algae

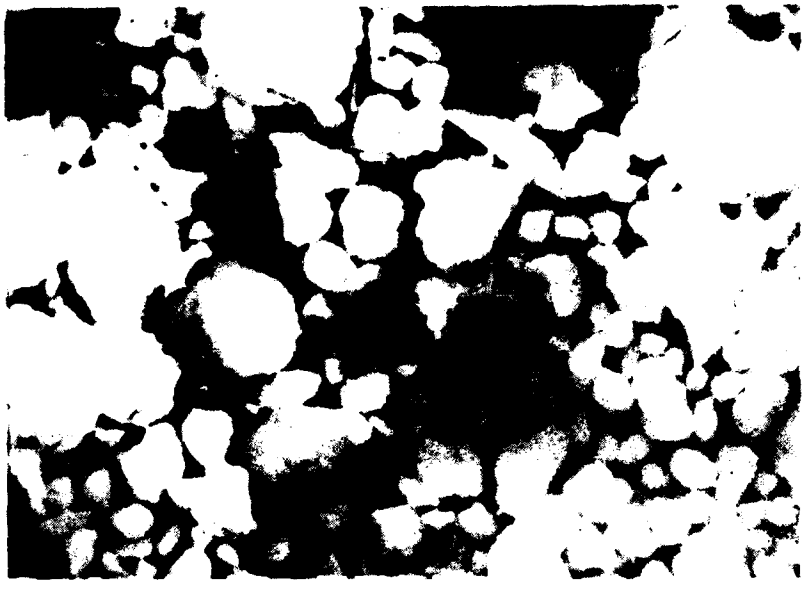

10KV X50 1000u 002 16425 NOL

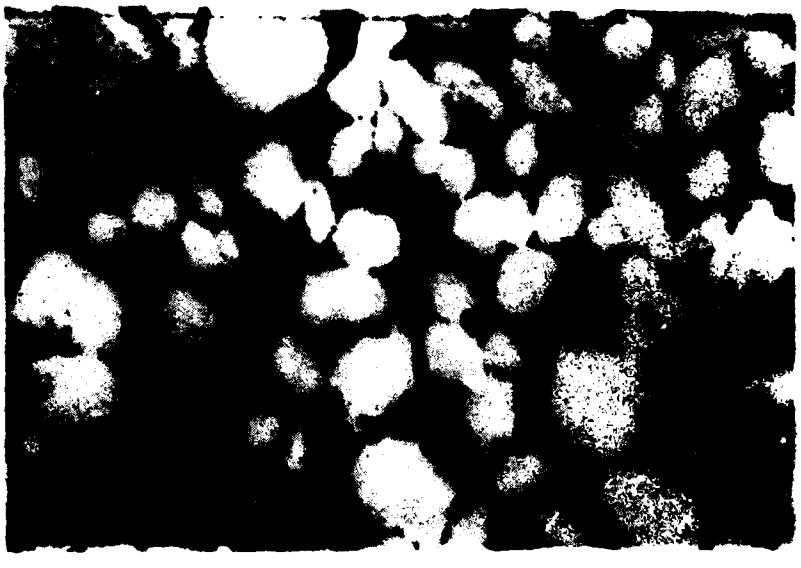

10KV X90 100u 002 10104 NOL

FIGURE 14. Photomicrographs of planktonic forams.

Top - A164-25, sand fraction

Bottom - C10-10, sand fraction (micritized)

amount of magnesian calcite in the silt-size fraction, however, the X-ray peak is so small that the presence or absence of magnesian calcite is a matter of judgment.

Sediment from V5-8 (observed by scanning electron microscopy, Fig. 15) is composed of planktonic and benthonic forams, small amounts of coral, molluscs, and red algae in the sand fraction. Skeletal constituents of V19-3 (Fig. 16) are primarily molluscs, planktonic and benthonic forams, red algae, bryozoans and Halimeda fragments. V7-65 is composed overwhelmingly of planktonic forams and molluscs in the sand fraction (Fig. 17). V5-5 contains bryozoans, molluscs, coral, planktonic forams, benthonic forams, echinoid fragments, Halimeda fragments and sponge spicules (Fig. 18). The clay-size fraction in all of these cores appears to be mainly coccoliths and unidentified shell fragments (Fig. 19).

Within these cores, calcite is contributed primarily by bryozoans, coral, planktonic forams, and coccoliths. Aragonite is contributed by molluscs and green algae (Halimeda). Magnesian calcite is contributed by benthonic forams, echinoid fragments, and red algae.

In order to locate magnesian calcite contributors not identified by scanning electron microscopy, thin sections, stained with Titan-yellow and fixed with 5 molar sodium hydroxide (Choquette and Trusell, 1978), were made of V19-3 and V5-8. The Titan-yellow preferentially stains magnesian calcite and corroborated the presence of magnesian calcite within these cores. The amounts of magnesian calcite (qualitative judgment) are small enough such that the magnesian calcite peak (2θ=29.81) must have been masked by the calcite peak (2θ=29.49) in the x-ray diffraction patterns.

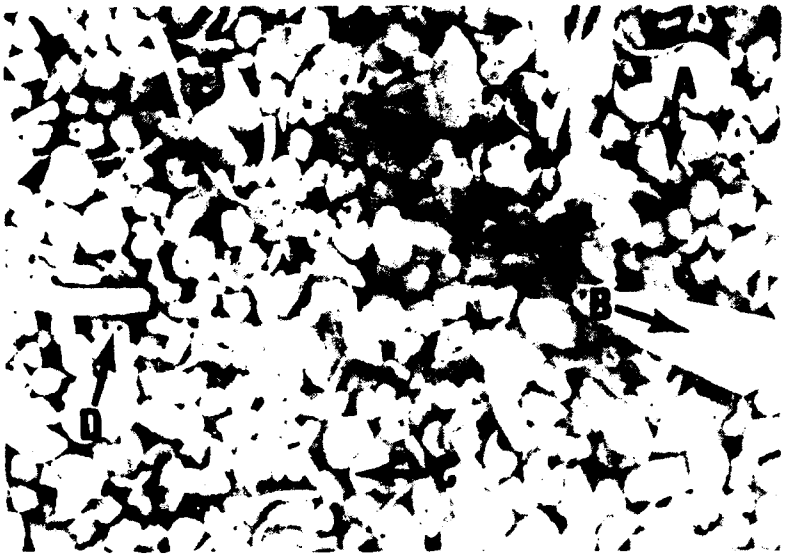

10KV X50 1000u 001 05080 NOL

FIGURE 15. Sand fraction of V5-8

A - planktonic foram C - benthonic foram

B - mollusc (pteropod) D - green algae (Halimeda)

10KV X50 1000u 006 01930 NOL

FIGURE 16. Sand fraction of V19-3

A - planktonic forams

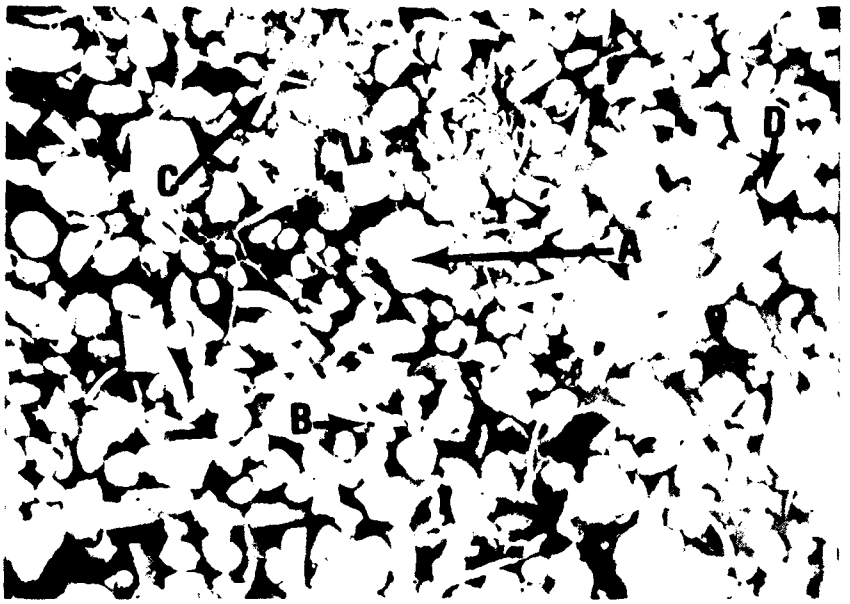

10KV X50 1000u 07650 NOL

FIGURE 17. Sand fraction of V7-65

A - planktonic forams
B - echinoid spine
C - coral (octocorallian spicule)
D - mollusc (pteropod fragment)

10KV X100 10011 002 05051 NOL

FIGURE 18. Sand fraction of V5-5

A - green algae (Halimeda)
B - sponge spicule
C - planktonic foram
D - bryozoan
E - echinoid spine

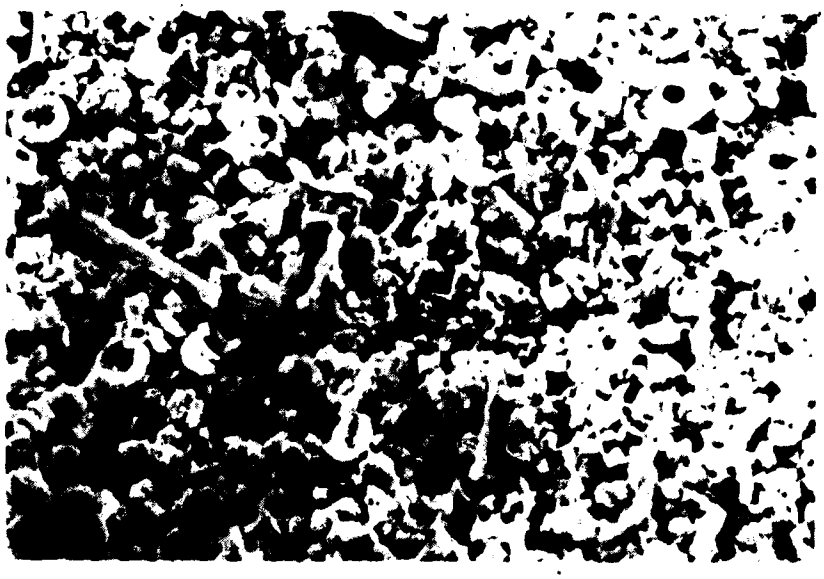

10KV X4000 10u 002 19030 NOL

10KV X5000 10u 002 16400 NOL

FIGURE 19. Coccoliths from clay-size fraction of V19-3 (top) and A164-25 (bottom)

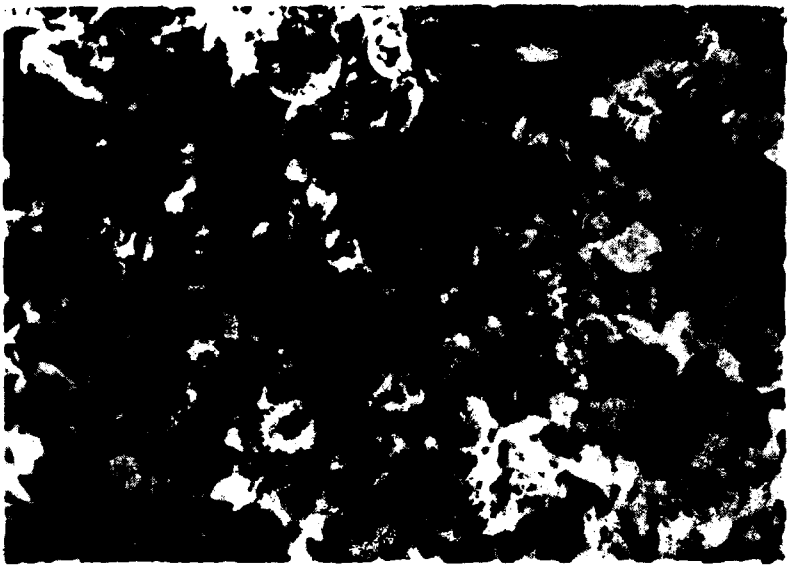

10KV X4000 10u 002 10104 NOL

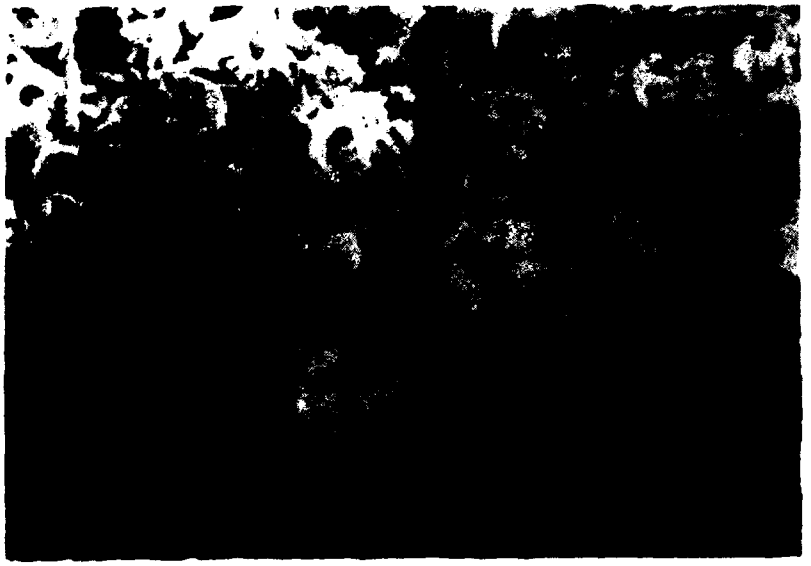

20KV X4000 10u 002 22610 NOL

FIGURE 19 (continued). Coccoliths from clay-size fraction of C10-10 (top) and C22-6 (bottom).

3. Cores containing calcite, aragonite and magnesian calcite:

The primary constituents of C22-5, C22-6, and C22-2, as identified by scanning electron microscopy (Figs. 20, 21, 22) appear to be planktonic forams and molluscs. Benthonic forams and red algae are present in smaller quantities (around 3%, Table 7). There are a large number of unidentified shell fragments in these cores (36%, 58%, and 32% respectively). The aragonite and calcite identified by x-ray can be easily accounted for by organisms present. Since the larger percentages of magnesian calcite (31%, 33% and 38% respectively) are more difficult to explain, thin sections were made of the sand fractions of the top intervals of these cores in an effort to determine source of magnesian calcite.

The unidentified shell fragments C22-5 were reexamined with a Kevex X7000 Energy Dispersive X-Ray Spectrometer (Kevex, Inc., Forest Hills, Calif.) to determine their elemental compositions. Most appear to be calcite or aragonite. Some of the fragments contain magnesium although the exact amounts cannot be determined with this system. When only magnesium and calcite are considered, magnesium, as percentage of combined weight, is present in quantities generally between 1 and 3%, although in one fragment, 15% magnesium was found.

Stained thin sections (Choquette and Trusell, 1978) were again used to determine the source of magnesian calcite. Red algae and echinoid fragments, identified in thin section, appear to be the primary contributors of the magnesian calcite (qualitative judgment). Magnesian calcite, however, was also present as intragranular cement in pores of planktonic forams and in algal borings similar to that found by

30KV X50 1000u 003 02260 NOL

FIGURE 20. Sand fraction of C22-6

A - planktonic foram

B - mollusc (gastropod fragment)

C - sponge spicule

D - benthonic forams

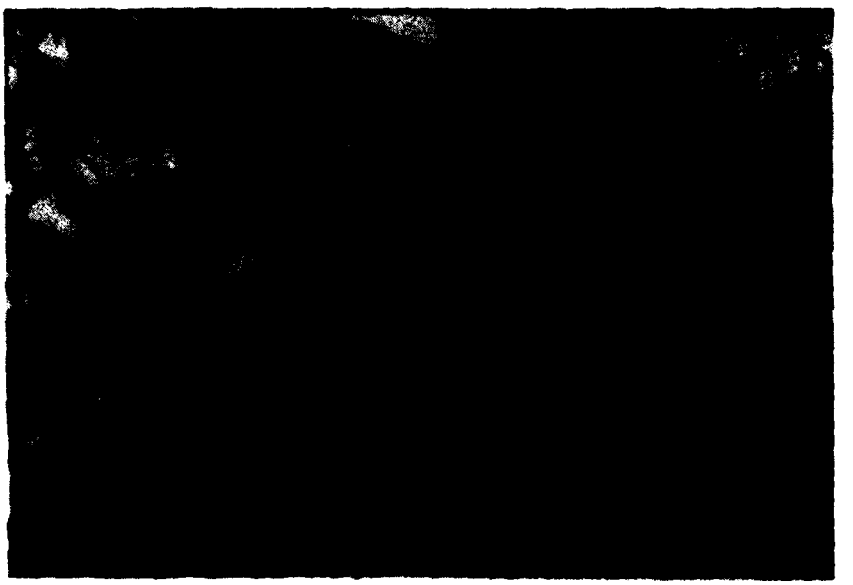

10KV X51 1000u 003 22055 NOL

FIGURE 21. Sand fraction of C22-5

A - planktonic foram

B - sponge spicule

C - mollusc (pteropod fragment)

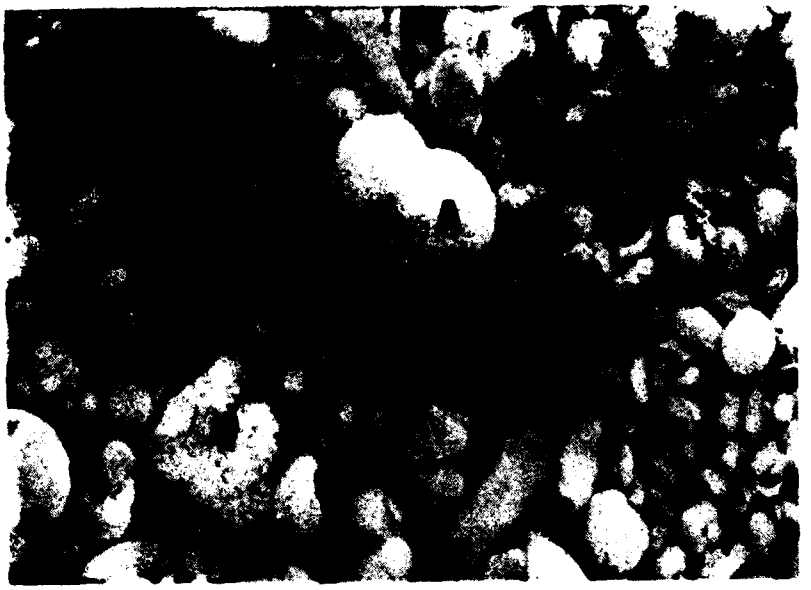

10KV X52 1000u 001 22020 NOL

FIGURE 22. Sand fraction of C22-2

A. planktonic foram

B. sponge spicule

C. coral (octocorallian spicule)

D. echinoid spine

E. mollusc (pteropod)

TABLE 7. SKELETAL CONSTITUENTS OF THE PEDESTAL CORES. ABSOLUTE NUMBERS ARE TO THE LEFT OF THE /, PERCENTAGES ARE TO THE RIGHT OF THE /.

Core	Bry #1$	Moll #1$	B.F.	P.F.	E.S.	Red Algae	S.S.	Ostra	Frags	Total
V5-5	21/4.5	65/13.8	15/3.2	51/10.8	36/7.6	27/5.7	41/8.7	-	215/45.6	471
C10-10	All micritized, probably all original pelagic forams, 1 ostracode									
C22-5	11/1.8	108/176	19/3.1	193/31.5	17/2.8	23/3.8	16/2.2	2/0.3	223/36.4	612
V5-8	1/.1	19/3.32	16/2.8	73/12.8	11/1.9	21/3.7	5/.08	-	426/74.5	572
C10-7	2/.04	40/8.6	14/3	87/18.6	23/4.9	22/4.7	27/5.8	-	252/54	467
C22-6	1/.05	12/3.8	7/3.8	34/18.7	5/2.7	13/7.1	4/2.2	-	107/58.8	453
C22-2	4/.08	40/88	11/2.4	197/43.5	23/5.1	12/2.6	21/3.9	-	145/32	453
C10-11	Almost all are pelagic forams (99$) plus fragments									
A164	Well micritized, looks as though all are pelagic forams									
V7-65	1/3	21/7.9	6/2.2	119/44.6	9/3.4	17/8	11/4.0	-	99/37.1	267
V19-3	4/2.1	8/4.1	4/2.1	47/242	-	36/18.6	4/2.1	-	91/34.9	194

Alexandersson and Milliman from the Brazilian shelf (1981). Finally, many of the sponge spicules were partially stained red indicating a magnesian calcite composition which had not been predicted from the scanning electron microscopy.

The one remaining pedestal core with aragonite, calcite, and magnesian calcite constituents, C10-7, also contains benthic forams, sponge spicules, and red algae in higher quantities than previous cores.

When mineralogy is plotted against depth, general trends can be observed. For example, when aragonite versus depth in meters is plotted (Fig. 23), the slight but definite trend of decreasing aragonite with increasing water depth is apparent. The cores with highest aragonite contents, V5-5, C22-5, V5-8, C10-7, C22-6, C22-2, V7-65 and V19-3, all contain molluscs. The three cores without aragonite contain no molluscs. The supposition can be made that molluscs are the primary contributors of aragonite on the pedestal.

Figure 23 also shows that there is a considerable amount of scatter. It is possible that aragonite is being contributed by different organisms at different water depths. However, aragonitic contributors such as coral and green algae appear to be as prevalent in V19-3 (4330 m) as in V5-5 (366 m). The probability is that the aragonite content is not being significantly affected by varying amounts of different contributors. Rather, factors such as dissolution and rapid burial may be more important.

Wilson (1975) states that in sea water aragonite is most soluble, then magnesian calcite, with low-magnesian calcite being the most stable. Thus, in a plot of depth versus calcite/calcite + magnesian

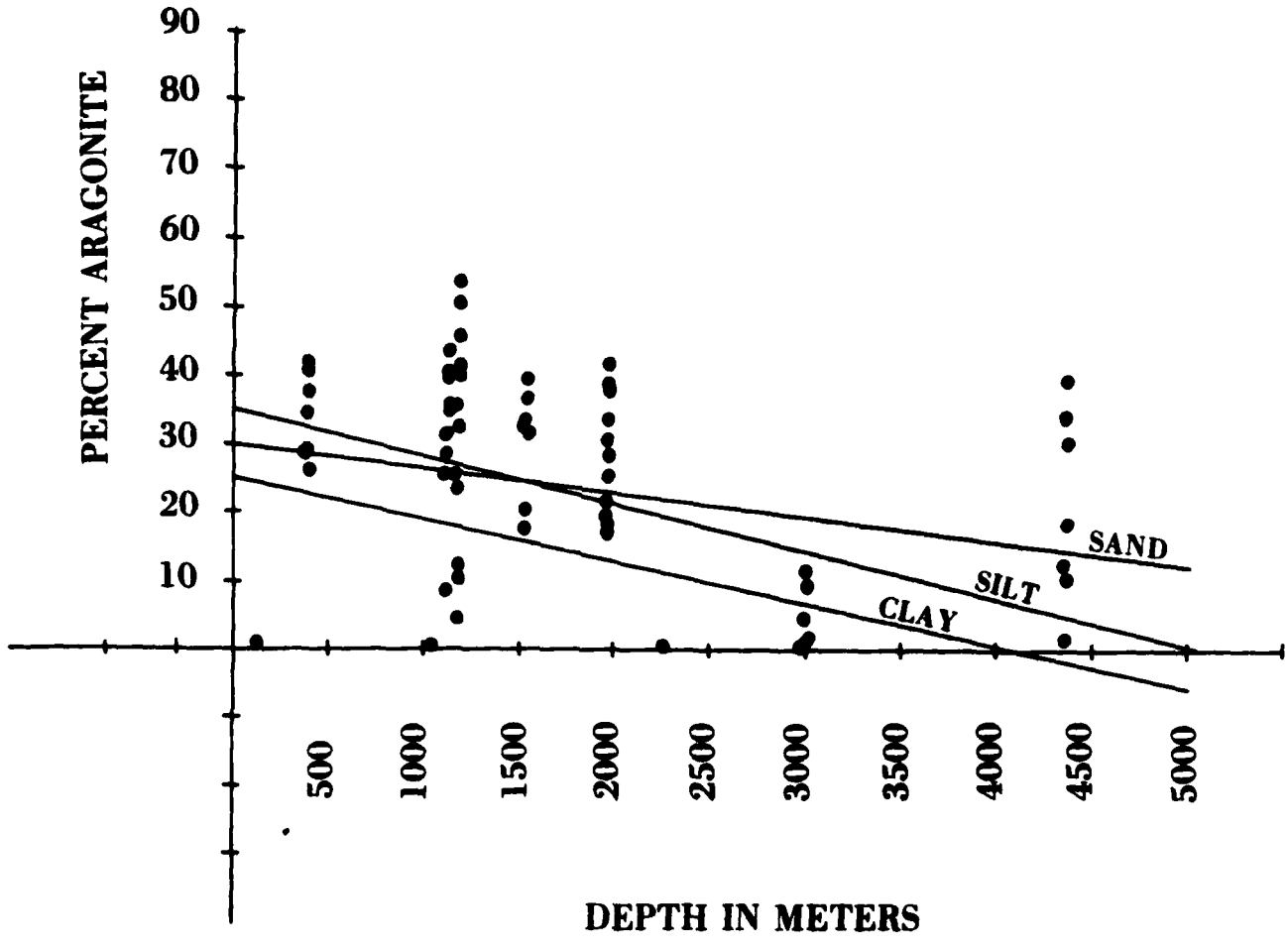

FIGURE 23. Aragonite content vs. water depth

calcite (Fig. 24), there is a distinct trend of increasing calcite as depth increases with lots of scatter. As the more soluble aragonite and magnesian calcite consituents begin to undergo dissolution earlier, the mineralogy of the deeper cores should be primarily calcitic. As the core depths increase, the percentage of calcite indeed becomes greater. Two deep cores, C10-11 and A164-25, are 100% calcite. However, the two deepest cores, V7-65 and V19-3, while containing high percentages of calcite, also contain over 10% aragonite in the sand and silt fractions. The aragonite lysocline is about 3000 m (Chen, 1964) in this area, the CCD about 4400-4500 m (Bowles, 1980). As with the previous plot, there is a large amount of scatter in the data. Again, the possibility exists that different organisms are significant contributors at different depths. However, planktonic forams, the most abundant contributors of calcite in these cores, make up equally significant portions of the shallow cores (V5-5, 11%) as they do in the deeper cores such as V19-3 (24%) and V7-65 (11.9%). V19-3 and V7-65 also contain molluscs, coral and red algae.

It is not possible to ignore the possibility that other variables are involved in the distribution of various minerals identified in the pedestal cores. Immediate burial is not a viable factor because the top intervals of the cores, presumably the sediments exposed to water, contain the same percentages as lower intervals. Rapid downslope transport of shallow-water carbonates is a possible variable. The slopes on the pedestal range from 30° to 13° to 2.8°, sufficient to encourage slipping or slumping if quantities of material begin to accumulate. It is known from unpublished Navy data (J. Matthews, personal communication) and

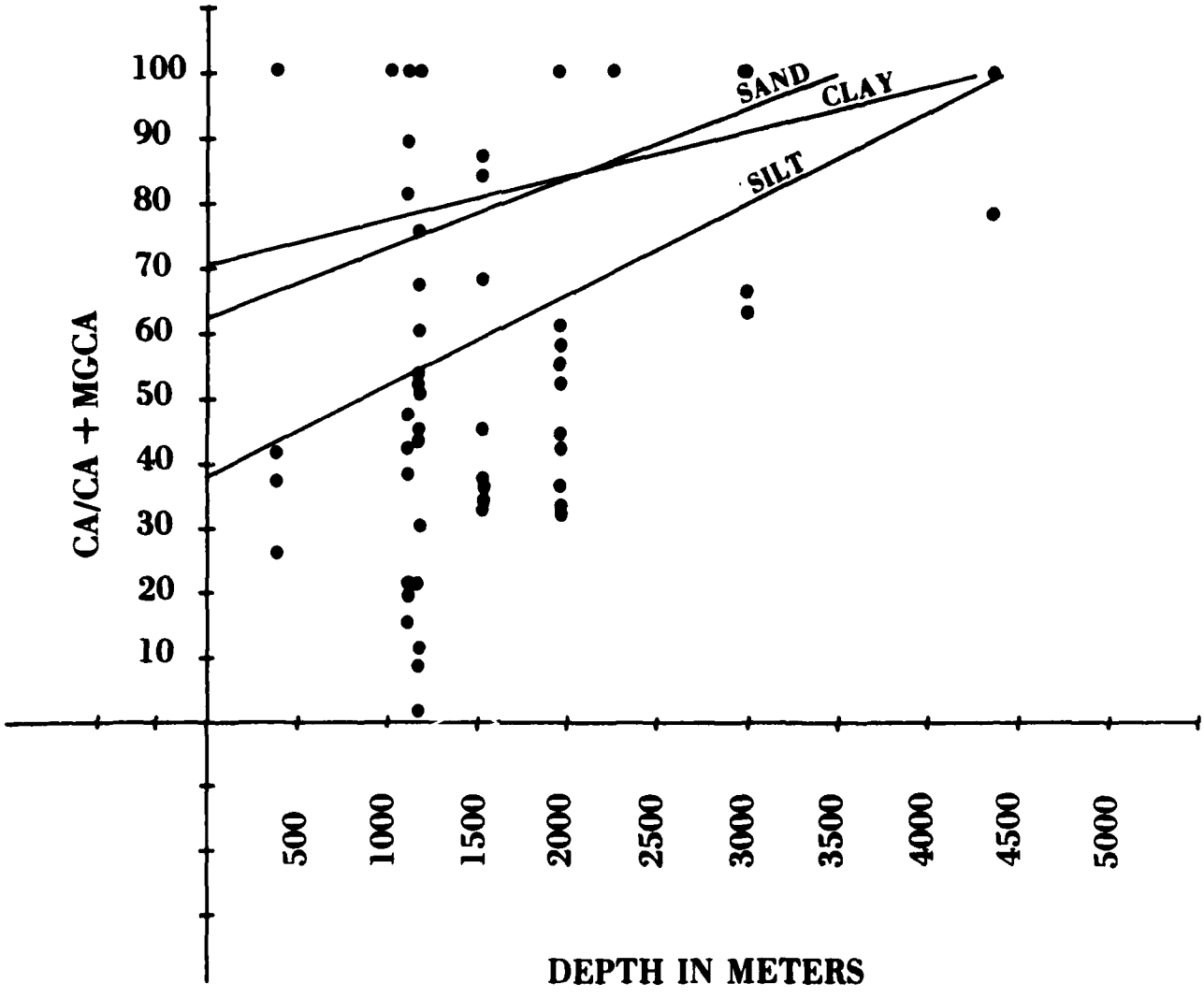

FIGURE 24. Calcite/calcite and magnesian calcite content vs. water depth.

Heezen and Hollister (1971) that current velocities in the area (both near the top of the pedestal and around the base) can be quite high. Although large amounts of sedimentary apron debris have not been identified from seismic profiles, there is evidence of some slumping (Appendix 5, B-B', C-C', and E-E'). Possibly some of the carbonate sediment being produced on the shallow platform is being rapidly transported down slope before dissolution can effectively occur, thus accounting for anomalously high quantities of aragonite and magnesian calcite at depths below where it would be expected.

Grain Size

Table 8 summarizes the grain-size data for the pedestal cores (with the exception of A164-25). Table 9 summarizes grain size data for the top intervals of the rise cores analyzed by NAVOCEANO. To make visualization easier, the percentages of sand versus depth have been plotted for the top 10-, 20-, and 30-cm intervals (Fig. 25). The correlation coefficients (R) range from -0.265 to -0.681 (Fig. 25). It is evident that the percentage of sand in all intervals within the cores decreases with increasing water depth. When data from the rise cores (NAVOCEANO) are combined with data from the pedestal cores, the same trend holds; the correlation coefficient is -0.310 (Fig. 26).

In plots of percentage of silt versus water depth for pedestal cores, there is a weak positive correlation for the top-, 10-, and 30-cm intervals (R = 0.125, 0.208, and 0.137 respectively). The correlation is more positive for the 20-cm interval (0.628, Fig. 07). When data from

TABLE 8. GRAIN SIZE DATA FOR PEDESTAL CORES

GRAIN SIZE DATA

Core	Interval	Sand	Silt	Clay
V5-5	-	-	-	-
	10	54.8	39.3	6.0
	20	77.0	20.6	1.7
	30	20.9	73.7	5.4
C10-10	top	35.1	38.7	26.2
	10	21.6	63.7	14.7
	20	33.0	56.9	10.0
	30	16.0	66.9	17.1
C22-5	top	69.2	25.9	4.9
	10	42.3	44.9	13.8
	20	17.0	67.7	15.3
	30	15.9	72.8	16.3
C10-7	top	41.2	35.5	23.3
	10	56.3	39.0	4.7
	20	60.7	35.2	4.0
	30	31.6	52.8	15.6
V5-8	top	11.0	36.9	52.2
	10	52.0	35.9	11.2
	20	79.2	18.0	2.0
	30	77.0	19.3	3.7
C22-6	top	30.6	19.5	39.9
	10	21.5	61.3	17.2
	20	61.8	34.5	3.6
	30	57.0	36.0	6.7
C22-2	top	37.8	35.0	27.0
	10	46.7	48.8	4.5
	20	43.3	48.0	8.6
	30	44.6	48.8	6.0
C10-11	top	26.0	54.1	20.0
	10	8.3	80.2	11.5
	20	6.8	81.9	11.3
	30	5.5	82.4	12.1
V7-65	top	41.5	43.4	14.8
	10	47.7	42.3	10.0
	20	11.5	77.8	10.6
	30	10.2	79.0	10.9
V19-3	top	4.8	31.4	63.8
	10	13.0	49.6	37.4
	20	6.3	71.2	22.5
	30	17.7	60.0	22.3

TABLE 9. GRAIN SIZE DATA FOR RISE CORES (NAVOCEANO)

RISE CORES

Core	Depth	Sand	Silt	Clay
K19-1R	4365	73.4	15.2	11.4
CG-18	4382	11.3	25.3	63.4
19-7	4410	72.9	16.9	10.1
K19-3	4490	.9	24.5	24.6
K19-4R	4520	37.3	28.7	38.0
K19-8	4555	6.8	18.1	75.1
K19-5	4620	3.7	31.1	65.2
K19-2	4425	10.6	19.2	70.2
K19-6	4620	21.3	36.6	42.0
Sta 3	4450	0	26.8	73.2

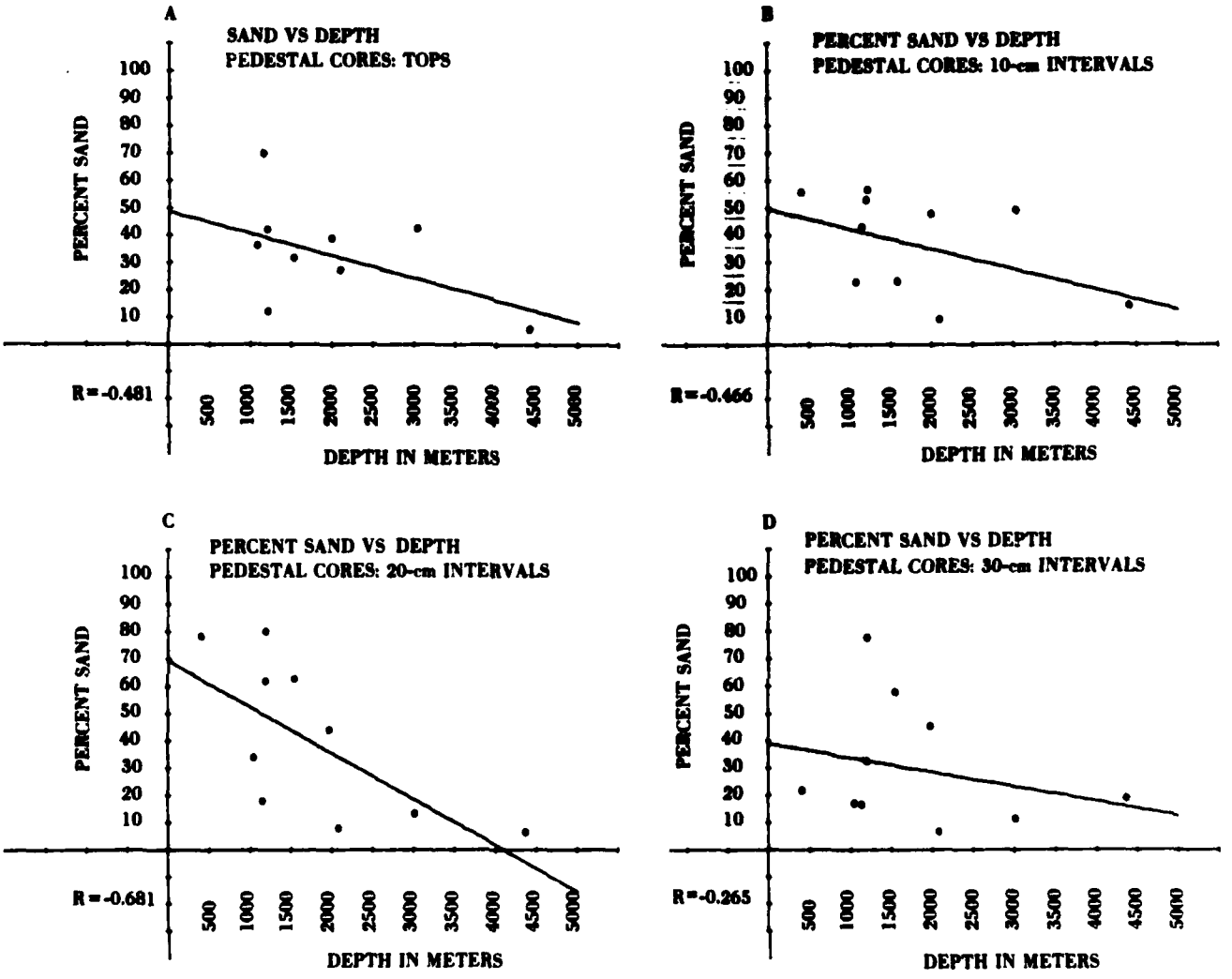

FIGURE 25. Percentage of sand vs. depth for the top, 10, 20, and 30 cm intervals of the pedestal cores.

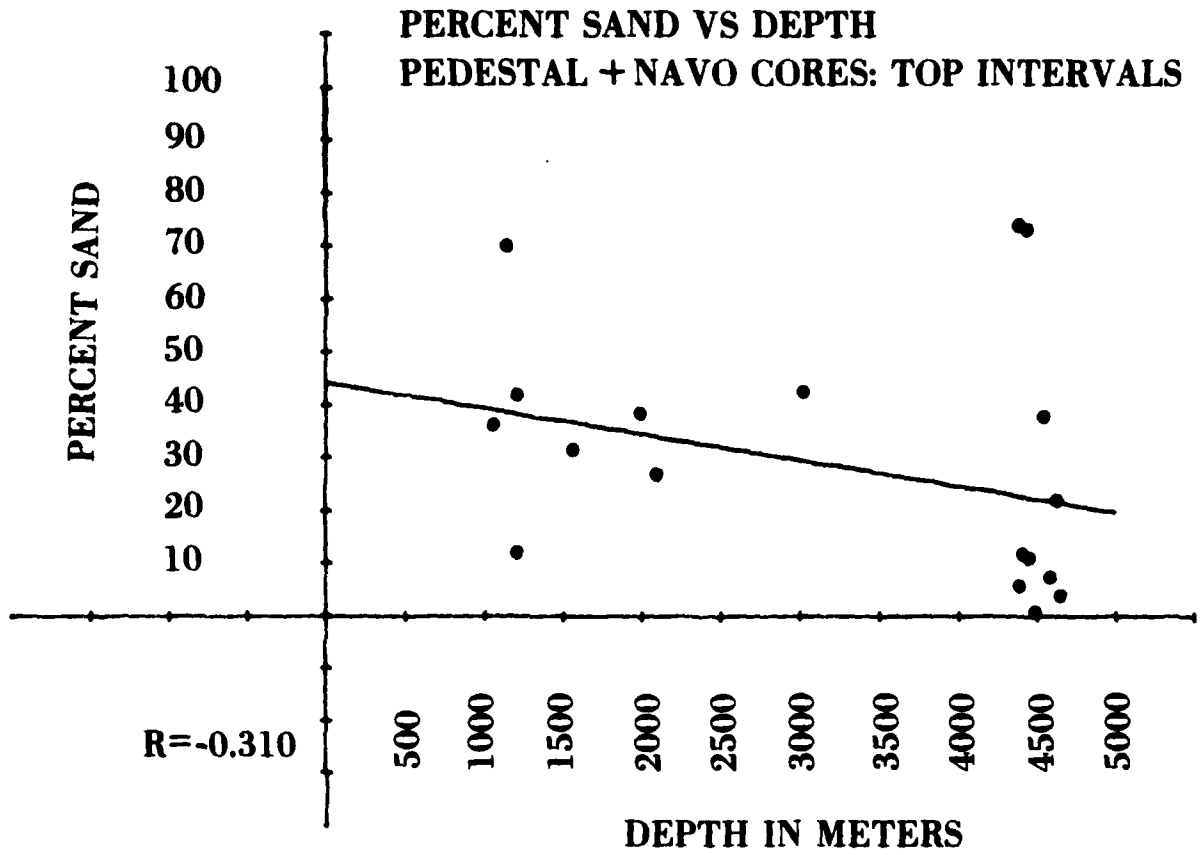

FIGURE 26. Combined pedestal and rise data: percent sand vs. water depth.

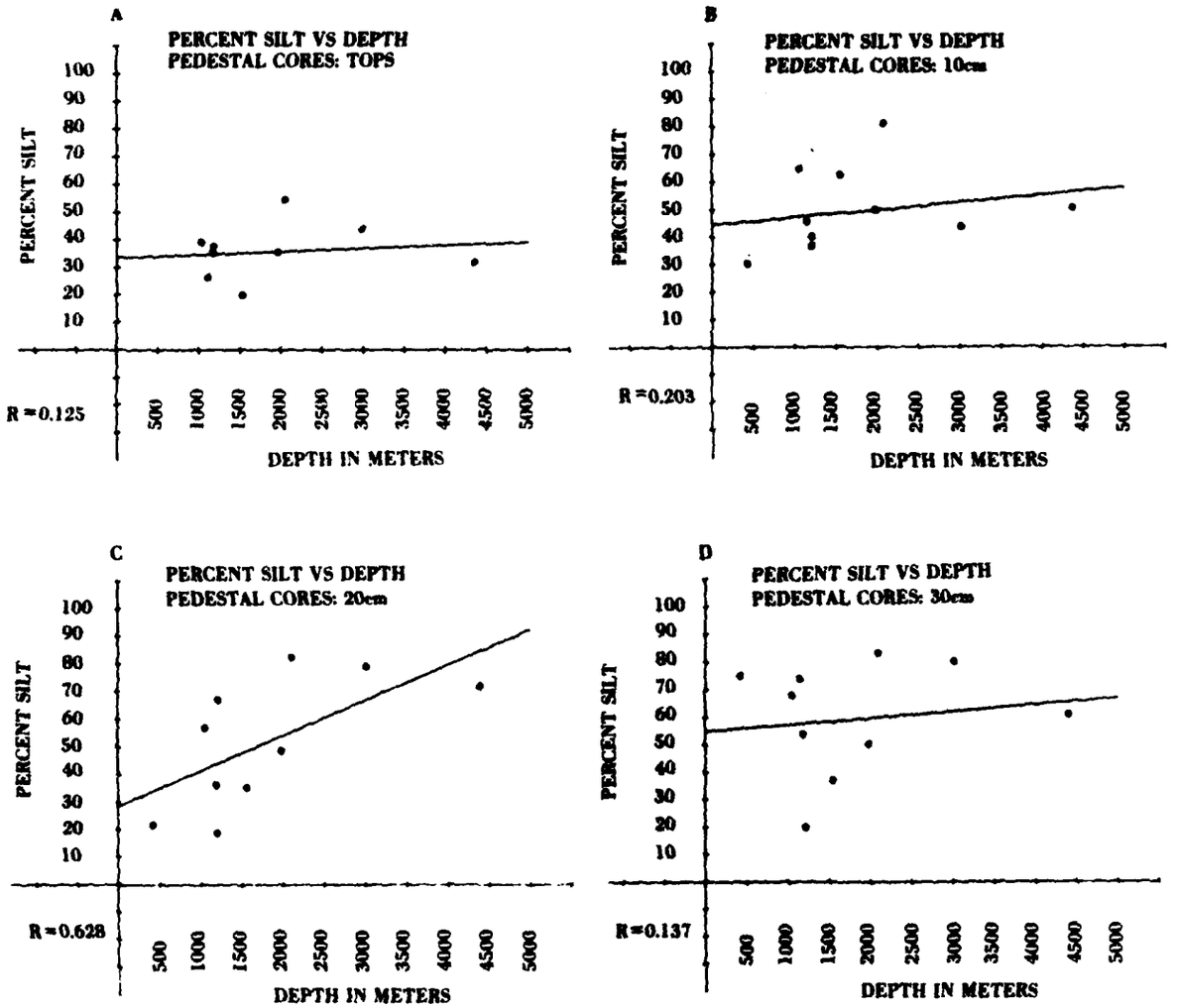

FIGURE 27. Percentage of silt vs. water depth for the top, 10, 20, and 30 cm intervals of pedestal cores.

the tops of pedestal cores are combined with data from the rise cores, the trend is reversed (Fig. 28). The correlation is -0.453 indicating that over the larger number of cores, the percentage of silt decreases with increasing water depth.

The percentage of clay increases with increasing water depth in all intervals of pedestal cores. This increase is shown when pedestal and rise core data are plotted together (Figs. 29 and 30). Correlation coefficients range between 0.441 and 0.775.

Figure 31, a schematic cross section of the pedestal, shows that the histograms of the grain-size distributions in the top intervals of each core are either unmodal or bimodal. For instance, the grain-size distribution of V5-5 (366 m) is dominated by a sand mode, 2.5Ø to 3.5Ø. The pedestal core at the distal end of the transect, V19-3, is also unimodal; however, the main mode is clay-sized, 8Ø. The top several cores including C10-10 and C22-5 are characterized by a main sand mode between 2.5Ø and 3.5Ø. There is, therefore, a preponderance of coarse-grained sediments until a depth of 1100 m is reached. Below 1100 m, grain size distributions change somewhat and cores are primarily characterized by bimodal distributions as illustrated by C10-7, C22-5, C22-2, and C10-11. These have a main sand mode between 2.5Ø and 3.5Ø and a clay mode around 8Ø to 9Ø. In C10-11, the finer mode is 6.5Ø to 7.5Ø or very fine silt size.

On Figure 19, V5-8 and V7-65 histograms are set below the pedestal to emphasize their deviation from the main pattern of grain size distribution. The main grain-size mode in the top cm of V7-65 is within the sand-size range (2.5Ø to 3.5Ø); a small clay-sized mode (8.5Ø to

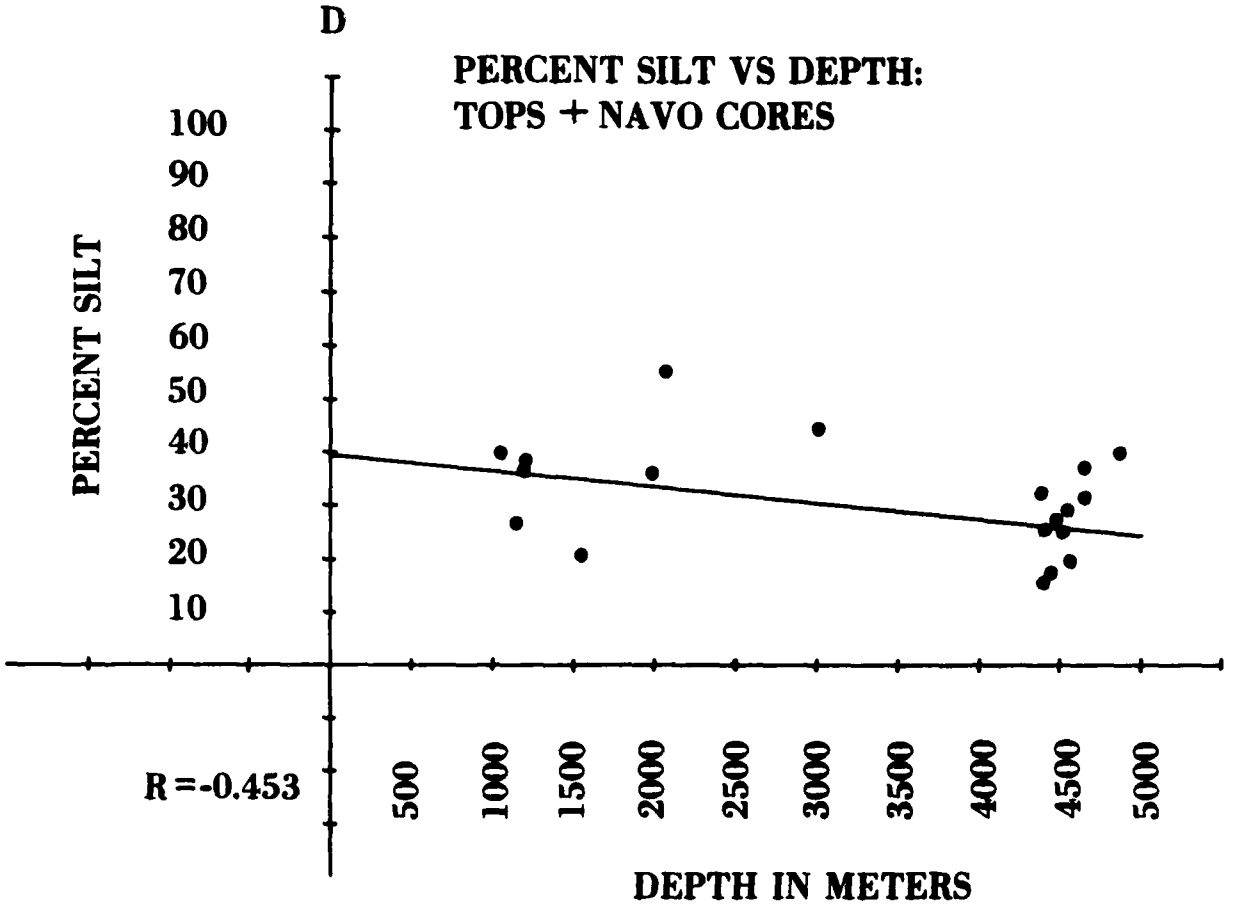

FIGURE 28. Combined pedestal and rise data: percent silt vs. water depth.

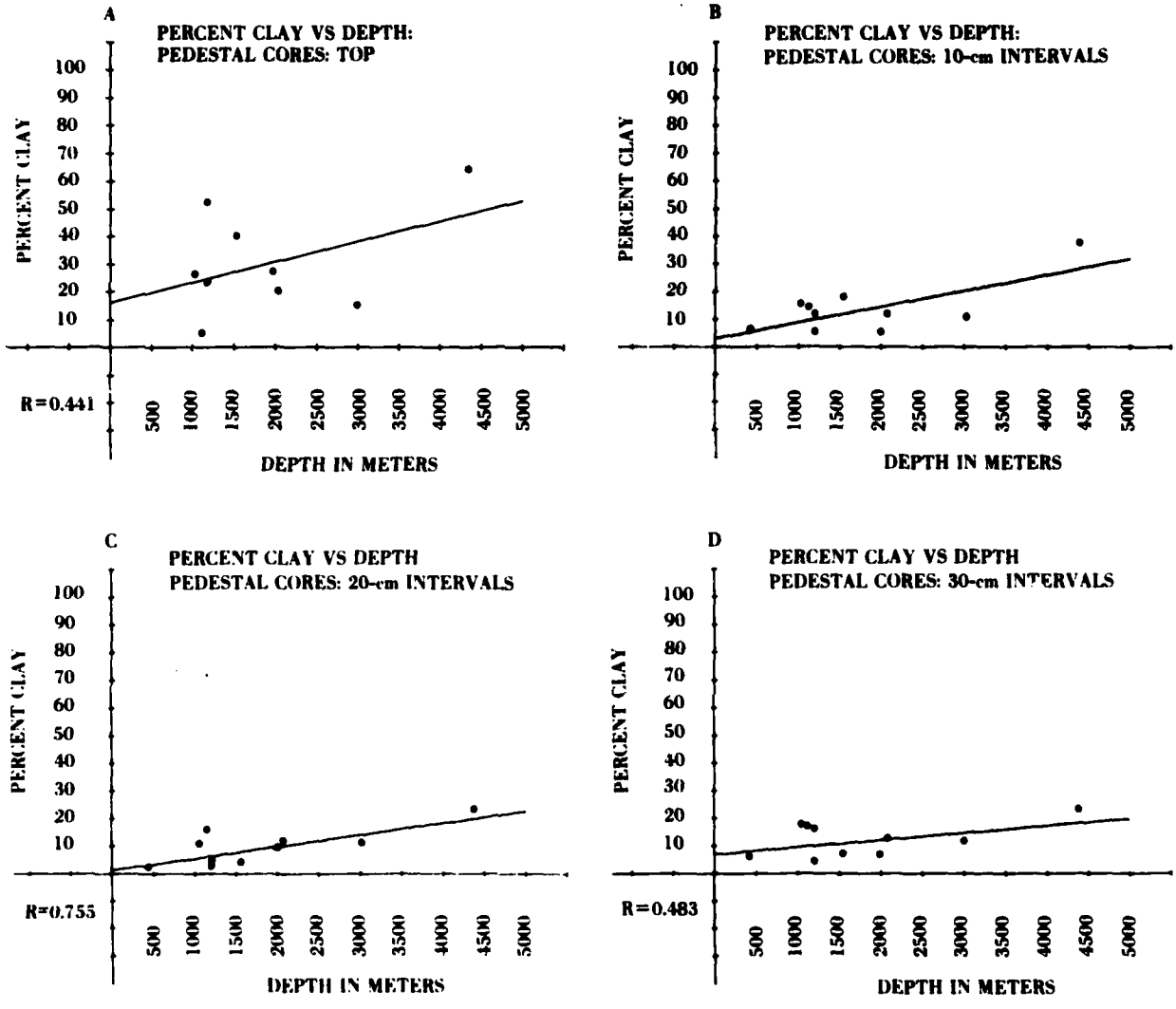

FIGURE 29. Percentage of clay vs. water depth for the top, 10, 20, and 30 cm intervals of the pedestal cores.

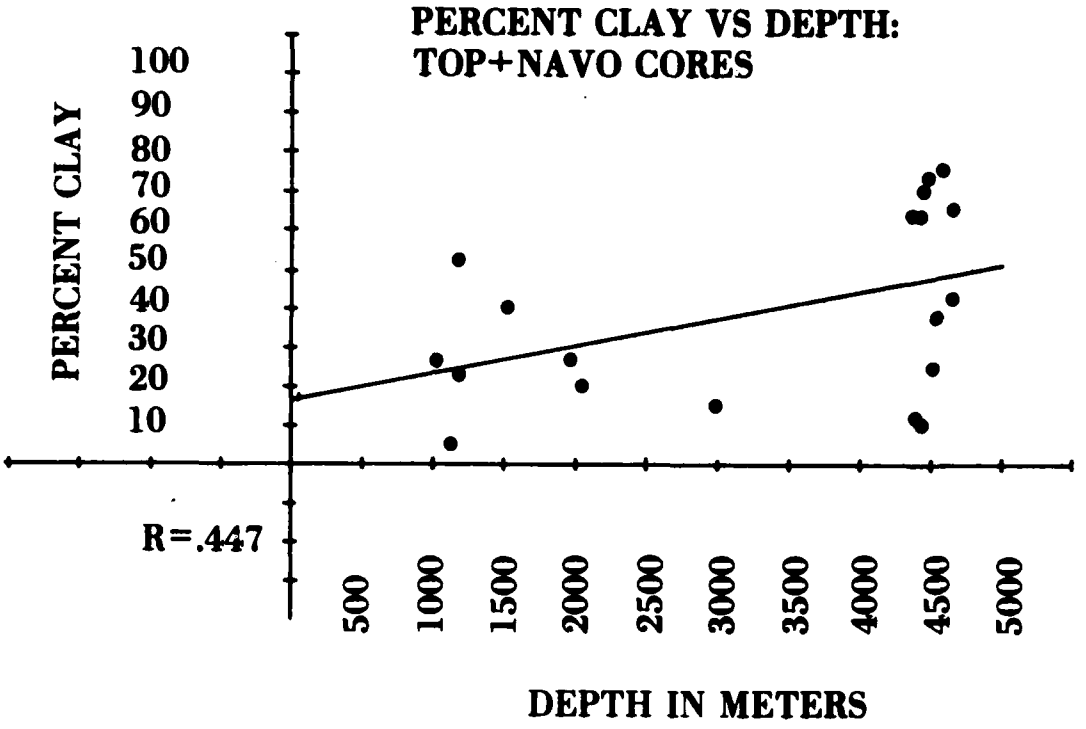

FIGURE 30. Combined pedestal and rise data: percent clay sized material vs. water depth.

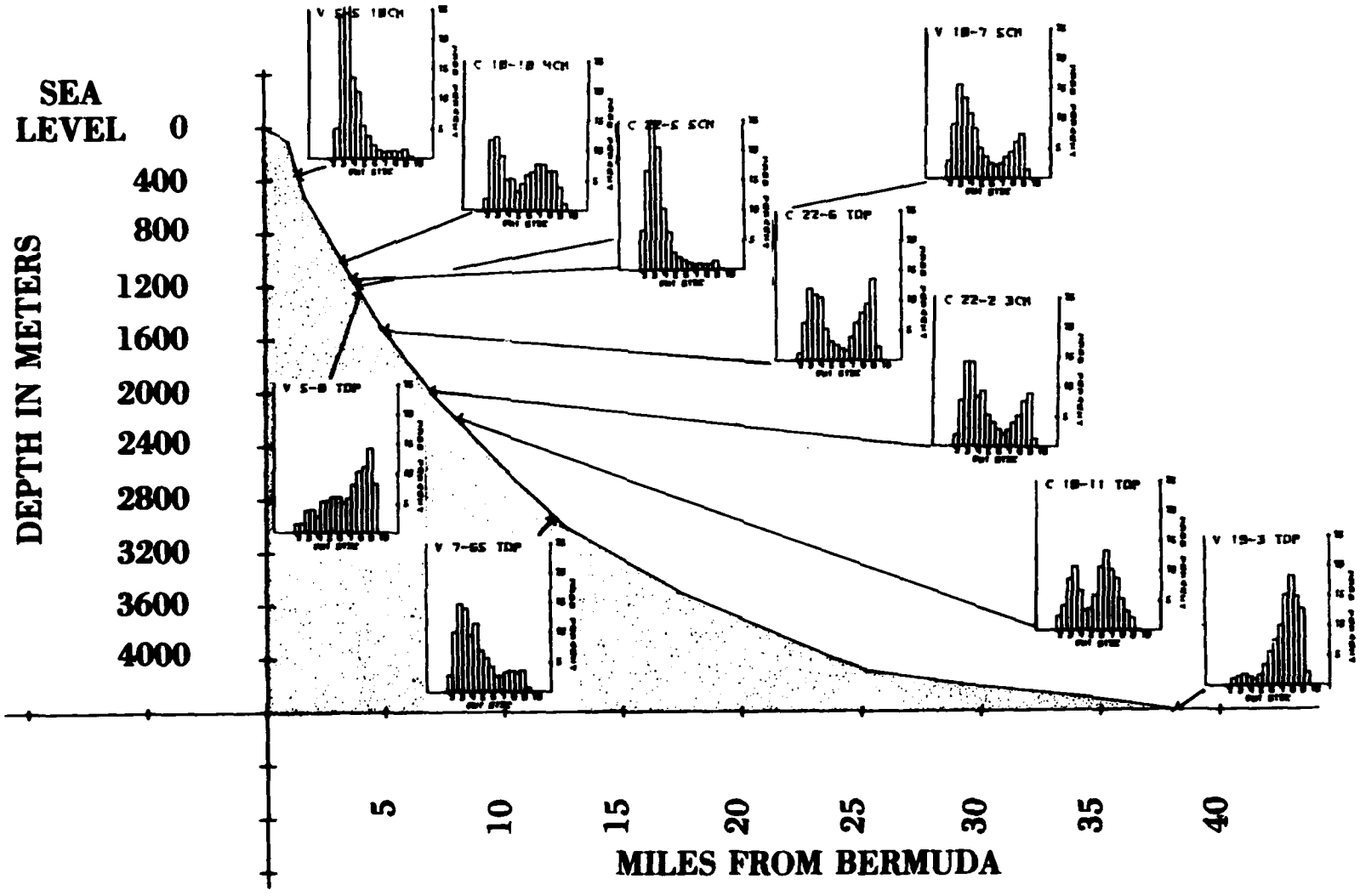

FIGURE 31. Schematic cross section of the Bermuda Pedestal. Cores were not actually recovered in a straight line so they are arranged on this cross section in order of depth.

9.5Ø) is present. Such large amounts (41%) of sand-sized sediment at this depth (2970 m) are unexpected. One would expect V5-8, recovered from a higher position on the pedestal (1150 m), to contain more sand-sized than clay-sized grains, yet the reverse is true.

Grain sizes for the different intervals within the same core vary considerably (Table 8). For example, in the shallow core V5-5, at the 10-, 20-, and 30-cm intervals, the percentage of sand varies between 55%, 77%, and 21%. The clay-sized fraction is small in all intervals (6%, 1.7%, and 5.4%). At 2094 m, C22-5 shows a marked decrease in the sand fraction (69%, 42%, 17%, and 16%) while the silt fraction increases (26%, 46%, 68%, and 73%). Similar variation among core intervals occurs in other cores. Within V5-8, for example, sand varies between 11%, 52%, 79%, and 77%; concurrently, silt decreases (37%, 36%, 2%, and 4%). In the deepest pedestal core, V19-3, sand is low in all intervals while the percentage of silt and clay varies considerably (Table 8).

Johnson et al. (1977) show evidence that on the Ontong Java Plateau mean grain size of sediments decreases at deposition sites primarily because of dissolution and fragmenting of calcareous microfossils. Determining the mean grain size is difficult for the Bermuda Pedestal cores since distributions of grain size are bimodal in many cases. In general, however, grain sizes are coarser at the top of the pedestal than the bottom or on the rise.

In the top intervals of the rise cores (NAVOCEANO), all taken within the same few hundred meters of water depth and roughly at the CCD, there is considerable variation. Sand varies between 0.9% and 73.4%. One of the main points, therefore, is that the highly variable

grain sizes in similar locations and within the same cores over small intervals indicate deposition cannot be occurring steadily. This same variability is also seen in the pedestal cores. It is likely, therefore, that deposition is discontinuous, with sediment being deposited episodically as slump material, tubidity deposits, etc. Material may also be resuspended by currents and eddies and be redeposited elsewhere on the Bermuda Apron and Rise. Such processes would account for the low correlation coefficients between grain size and water depth.

SUMMARY AND CONCLUSIONS

The variables examined in this study are:

1. location on the pedestal, i.e., water depth
2. total carbonate content
3. constituent grains
4. bulk-sample carbonate mineralogy
5. grain size

The relationships between these variables are complex, but a few general statements can be made. There is an overall relationship between water depth and all the other variables. Total carbonate content generally decreases with increasing water depth. The percentage of aragonite and magnesian calcite declines with increasing water depth. The types of constituent particles present are related to water depth. In shallower depths, there are a variety of organisms present. With increasing water depth, fewer types of organisms are present. Planktonic forams become more prevalent with deeper water and shallow-water reef debris becomes less prevalent. Grain size generally becomes smaller with increasing water depth. Other relationships among variables follow:

1. Grain size and constituent particles: Pelagic forams are almost always sand size and compose the bulk of the sand modes (SEM examination).

2. Grain size and total carbonate: As total carbonate decreases, so does grain size; whether this was due to greater contributions of clay minerals or due to dissolution of carbonate sediment could not be determined with the samples available. Since the clay-sized fractions

contained appreciable numbers of coccoliths, the size decrease may be related to the constituent grains.

3. Constituent particles and mineralogy: Constituent grains correlate well with mineralogy. Planktonic forams are the major contributors of calcite, molluses and Halimeda are the major contributors of aragonite, and red algae and echinoid fragments are the major contributors of magnesian calcite.

While these trends are present, they are often overlain by high variability in the data. Correlation coefficients are generally weak. This variability and scatter indicate that sediment types and distribution on the pedestal may not be controlled by sedimentation rates; turbidity currents and slumping play an important role in sediment distribution on the pedestal and apron.

The sediments on the Bermuda Pedestal are significantly different from sediments on the rise. Whereas sediments on the rise are almost entirely nanofossil oozes with a high clay mineral content, sediments on the pedestal are almost entirely carbonate with very little clay mineral content. Sediments on the pedestal are a combination of material deposited from the platform such as red algae, Halimeda, sponge spicules, bryozoan and coral particles, and pelagic material such as ostracods, coccoliths, and planktonic forams. There are also a host of benthic organisms such as molluscs, echinoids, and benthic forams which may be indigenous to the area from which they were recovered. Organisms indigenous to shallow reef areas were found at great depths on the pedestal (around the CCD and below), indicating that rapid, downslope transport must have occurred.

The distribution of these sediments on the Bermuda Pedestal is largely controlled by the bathymetry of the area. Seismic profiles indicate sparse sediment cover on the pedestal and much thicker cover on the apron and rise. Sediment thickness, as detected by seismic profiles, ranges from the pinchout near the base of the pedestal to greater than 900 m on the rise near DSDP Site 386. Batyhymetry shows extremely steep slopes (30°) on the upper reaches of the pedestal and gentler slopes (2.8-3.5°) on the apron where sediment is accumulating. There is also evidence of some slumping and turbidity flows, which supports the hypothesis that sediment is being transported down the seamount by these processes.

Finally, currents may also play a part in the distribution of sediments. Strong currents on the pedestal may encourage the initiation of transport, and currents on the apron and rise may resuspend and redistribute sediments from these areas.

REFERENCES

Alexandersson, E.T. and J. D. Milliman (1981). Intragranular Mg-Calcite Cement in Halimeda Plates from the Brazilian Continental Shelf. Journal of Sedimentary Petrology, v. 51, No. 4, p. 1309-1314.

Bathurst, R.G.C. (1971). Carbonate Sediments and Their Diagenesis: Elsevier Scientific Publishing Co., New York, 658 p.

Bialek, E.L. (1966). Handbook of Oceanographic Tables, Matthews Tables, Table 11, U.S. Naval Oceanographic Office, Washington, D.C. p. 63-96.

Bowles, F.A. (1975). Geology/Geophysics near Bermuda. In: Physical Environmental Scenario for the Near Bermuda Area. Ocean Engineering and Construction Project Office (FPO-1), Chesapeake Div., Naval Facilities Engineering Command, Washington, D.C. p. B-1-12 - B-1-21.

Bowles, F. A. (1979). II. Site Survey, DSDP Site 386, Initial Reports of the Deep Sea Drilling Project. ed. Ansis Kaneps, v. XIII, U.S. Government Printing Office, Washington, D.C., v. 43, p. 1013-1017.

Bowles, F. A. (1980). Stratigraphy and Sedimentation of the Archipelagic Apron and Adjoining Area Southeast of Bermuda. Marine Geology, v. 37, p. 267-294.

Bowles, F. A., E. A. Angino, J. W. Hosterman, and O. K. Galle (1971). Precipitation of Deep-Sea Palygorskite and Sepiolite. Earth and Planetary Science Letters, v. 11, p. 324-332.

Chen, C. (1964). Pteropod Ooze from Bermuda Pedestal. Science, v. 144, No. 3614, p. 60-62.

Chocquette, P. W. and F. C. Trusell (1978). A Procedure for Making the Titan-Yellow Stain for Mg-Calcite Permanent. Journal of Sedimentary Petrology, v. 48, p. 639-646.

Cotton, C. A. (1969). The Pedestals of Oceanic Volcanic Islands. Geological Society of American Bulletin, v. 80, p. 749-760.

Damuth, J. E. (1975). Echo Character of the Western Equatorial Atlantic Floor and Its Relationship to the Dispersal and Distribution of Terrigenous Sediments. Marine Geology, v. 18, p. 17-45.

Damuth, J. E. (1980). Use of High-Frequency (3.5-12 kHz) Echograms in the Study of Near-Bottom Sedimentation Processes in the Deep-Sea: A Review. Marine Geology, v. 38, p. 51-75.

DSDP (1978). Initial Reports of the Deep Sea Drilling Project, Volume 43. US Government Printing Office, Washington, DC.

DSDP (1979). Initial Reports of the Deep Sea Drilling Project, Volume 43. US Government Printing Office, Washington, DC, p. 195-321.

Folk, R. L. (1974). Petrology of Sedimentary Rocks. Hemphill Publishing Company, Austin, Texas, 182 pp.

Gees, R. A. and F. Medioli (1970). A Continuous Seismic Survey of the Bermuda Platform, Part I: Castle Harbour. Maritime Sediments, v. 6, No. 1, p. 21-25.

Ginsberg, R. N. and J. H. Schroeder (1973). Growth and Submarine Fossilization of Algal Cup Reefs, Bermuda. Sedimentology, p. 575-614.

Heezen, B. C. and C. D. Hollister (1971). The Face of the Deep. Oxford University Press, Inc., New York, N.Y., 658 p.

Holcombe, T. L. and B. C. Heezen (1970). Patterns of Relative Relief, Slope and Topographic Texture in the North Atlantic Ocean. Technical Report No. 8, Cu-8-70, Naval Ship Systems Command N00024-67-1186, Lamont-Doherty Geological Observatory, Columbia University, Palisades, N.Y., 127 p.

Hulsemann, J. (1966). On the Routine Analysis of Carbonates in Unconsolidated Sediments. Journal of Sedimentary Petrology, v. 36, No. 24, p. 622-625.

Huang, T. C. and J. W. Pierce (1971). The Carbonate Minerals of Deep Sea Bioclastic Turbidites, Southern Blake Plateau. Journal of Sedimentary Petrology, v. 41, No. 1, p. 251-260.

Hyndman, R. D., G. K. Mueche and F. Aumento (1974). Deep Drill 1972, Heat Flow and Heat Production in Bermuda. Canadian Journal of Earth Science, p. 809-818.

Johnson, R. C., E. L. Hamilton and W. H. Berger (1977). Physical Properties of Calcareous Ooze: Control by Dissolution at Depth. Marine Geology, v. 24, p. 259-277.

Jordan, C. F., Jr. (1971). Bioclastic Sediment Dispersion Off Bermudan Patch Reefs. American Association of Petroleum Geologists Bulletin, v. 55, pt. 1, p. 346.

Kelley, J. T. (1981). Size Distribution of Disaggregated Inorganic Suspended Sediment: Southern New Jersey Inner Continental Shelf. Journal of Sedimentary Perology, v. 51, No. 4, p. 1097-1102.

Laine, E. P. (1979). Geologic Effects of the Gulf Stream System in the North American Basin, PhD Thesis, MIT and Woods Hole Oceanographic Institute, (Unpub.), 164 pp.

Laine, E. P. and C. D. Hollister (1981). Geological Effects of the Gulf Stream System on the Northern Bermuda Rise. Marine Geology, v. 39, p. 277-310.

Land, L. S. and Mackenzie (1970). Field Guide to Bermuda Geology. Bermuda Biological Station for Research, Special Publication No. 4, St. George's West, Bermuda, 14 pp.

McGregor, B., P. Betzer and D. Krause (1973). Sediments in the Atlantic Corner Seamounts: Control by Topography, Paleowinds, and Geochemically Detected Bottom Currents. Marine Geology, v. 14, p. 179-190.

Milliman, J.D. (1974). Marine Carbonates. Springer-Verlag, New York, N.Y., 374 pp.

Naval Weather Service Command (1974). Bermuda Environmental Scenario. Naval Weather Service, Asheville, N.C., 199 pp.

Neumann, C. A. (1965). Processes of Recent Carbonate Sedimentation in Harrington Sound, Bermuda. Bulletin of Marine Science, v. 15, No. 4, p. 987-1035.

Pirsson, L. V. (1914). Geology of Bermuda Island: The Igenous Platform. American Journal of Science, v. 38, p. 777-808.

Reynolds, P. H. and F. Aumento (1974). Deep Drill, 1972, Potassium-Argon Dating of the Bermuda Drill Core. Canadian Journal of Earth Science, v. 11, p. 1269-1273.

Schmitz, J., Jr. (1977). On the Deep General Circulation in the Western North Atlantic, Journal of Marine Research, v. 35, No. 1, p. 21-35.

Stanley, D. J. and D. J. P. Swift (1967). Bermuda's Southern Aeolianite Reef Tract. Science, v. 157, No. 3789, p. 677-681.

Stanley, D. J. and D. J. P. Swift (1968). Bermuda's Reef-Front Platform: Bathymetry and Significance. Marine Geology, v. 6, p. 479-500.

Stanley, D. J. and P. T. Taylor (1977). Sediment Transport Down a Seamount Flank by a Combined Current and Gravity Process. Marine Geology, v. 23, p. 77-88.

Tucholke, B. (1979). Relationships Between Acoustic Stratigraphy and Lithostratigraphy in the Western North Atlantic Basin, in Initial Reports of the Deep Sea Drilling Project, v. XLIII, ed. Ansis Kaneps. U.S. Government Printing Office, Washington, D.C. p. 827-846.

Vogt, P. R., G. L. Johnson, T. L. Holcombe, T. G. Gilg and O. E. Avery (1971). Episodes of Seafloor Spreading as Recorded in the North Atlantic Basement. Tectonophysics, v. 12, p. 211-234.

Vogt, P. and A. Ballard (1976). The Bermuda Discontinuity (known as the "J-Anomaly") Between New England Seamounts and Southeastern End of Grand Banks, Sites 43-6, 43-7, 44-4, 44-5. Abstracts of the Annual Meeting of the American Geophysical Union, Washington, DC.

Vogt, P. and A. Einwich (1979). Magnetic Anomalies and Seafloor Spreading in the Western North Atlantic, and a Revised Calibration of the Keathly (M) Geomagnetic Reversal Chronology, in Initial Reports of the Deep Sea Drilling, Project, v. XLIII, ed Ansis Kaneps. U. S. Government Printing Office, Washington, D.C. p. 847-856.

Weast, R. C. ed. (1964). Handbook of Chemistry and Physics, 45th Ed. Chemical Rubber Publishing Co., Cleveland, Ohio, p. 124, Section D.

Wilson, J. L. (1975). Carbonate Facies in Geologic History, Springer-Verlag, Berlin, 471 pp.

APPENDICES

APPENDIX 1. Ship tracks used in compiling Bermuda bathymetry (plotted).

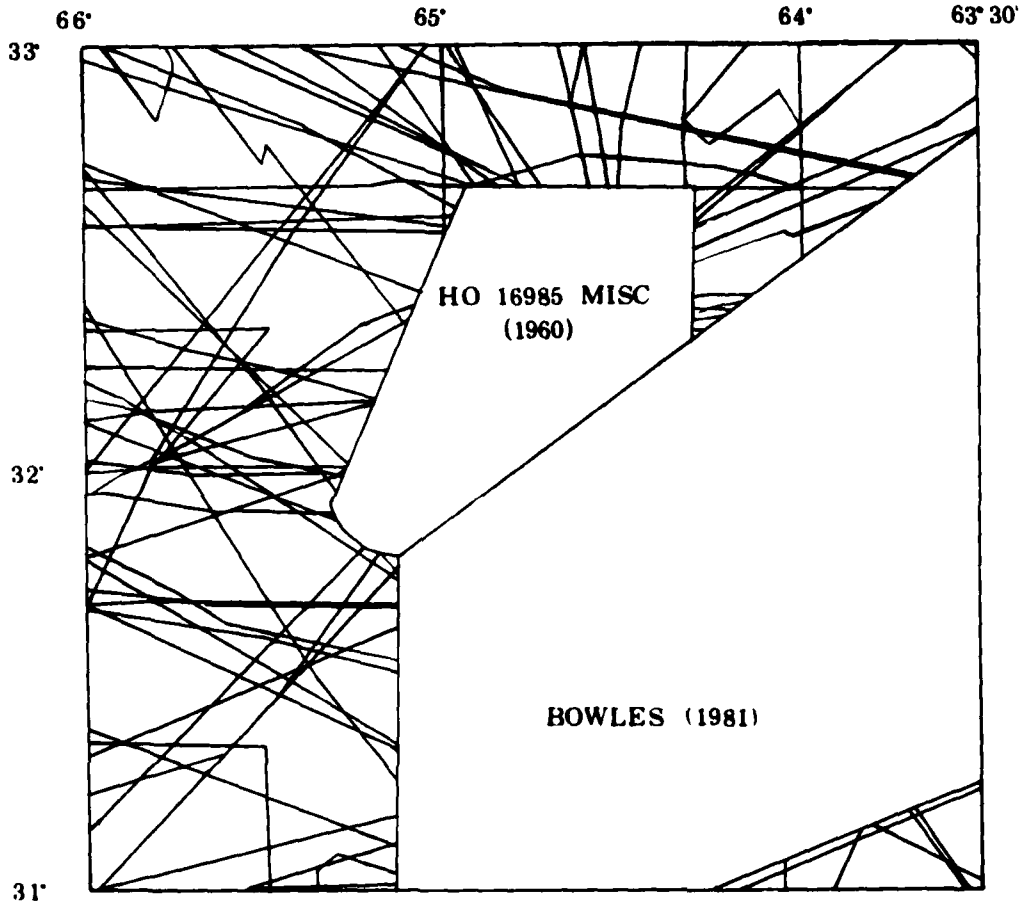

APPENDIX 2. SHIP TRACKS USED IN COMPILING BERMUDA BATHYMETRY (LISTED)

SHIP TRACKS

Keathley	V1818
TAG 70	V1802
C2116	C1001
C2110	V1801
C2102	C1101
C2101	V1702
Ka70A	V1701
Ka68J(?)	DSDP43GC
KA68D	W1343513
KA68C	W1343510
LY70F	DA344602
E3J78	V2101
V3108	V2603
V3107	V2602
C1906	V2601
CH057L01	V2807
A2042L06	V2806
V2503	V2805
V2307	V2610
V2306	V2609
V2013	
V2012	
C1601	
C1510	
V1902	
V1901	
V1819	

APPENDIX 3. Location of seismic profiles used to plot post-Horizon A sediment "pinch-out".

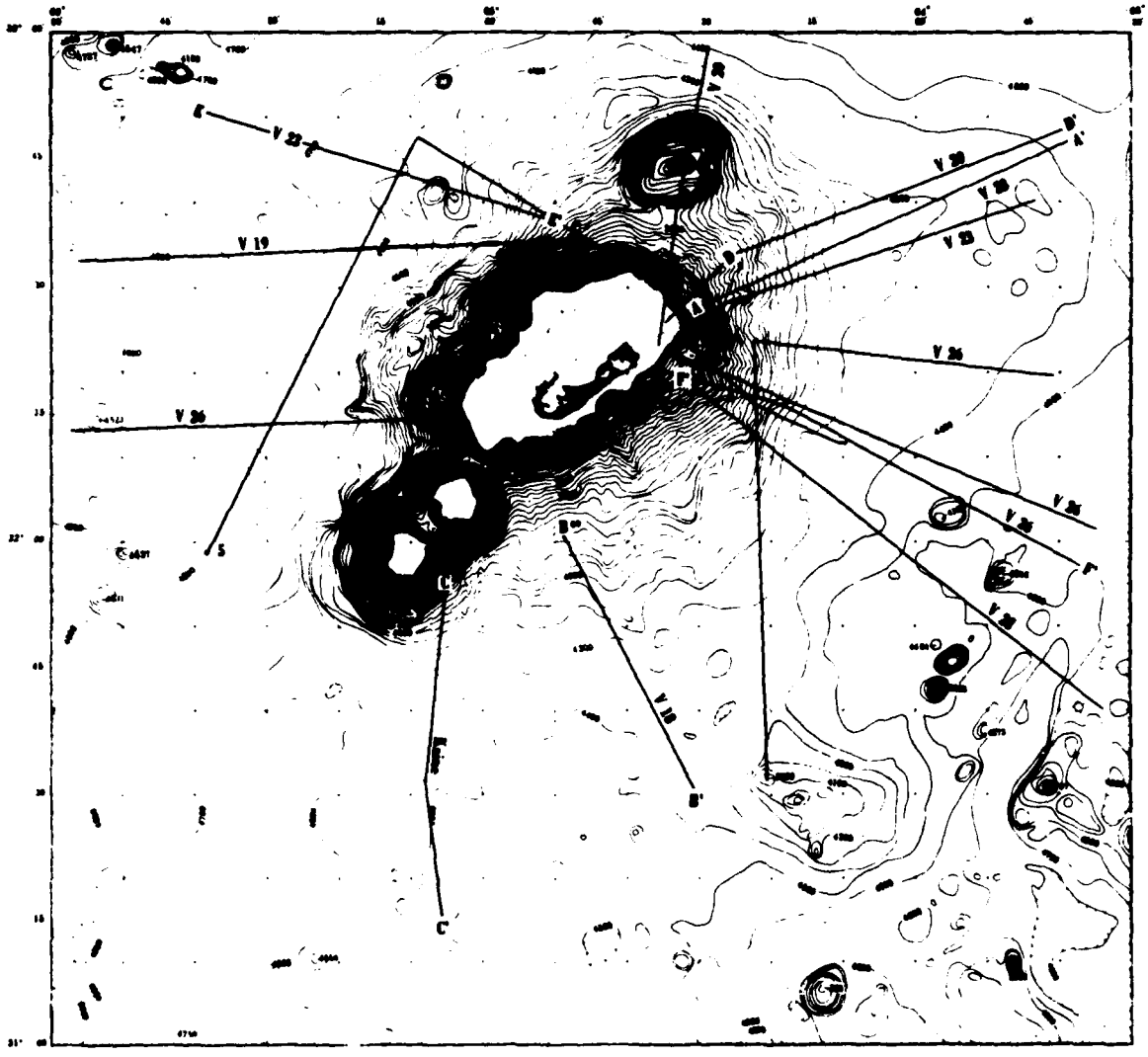

APPENDIX 4. VAPOR PRESSURE OF WATER USED TO COMPUTE BAROMETRIC PRESSURE FOR THE CARBONATE ANALYSES

	0.0	0.2	0.4	0.6	0.8
15	12.788	12.953	13.121	13.290	13.461
16	13.634	13.809	13.987	14.166	14.347
17	14.530	14.715	14.903	15.092	15.284
18	15.477	15.6731	15.871	16.071	16.272
19	16.477	16.685	16.894	17.105	17.319
20	17.535	17.753	17.974	18.197	18.422
21	18.650	18.880	19.113	19.349	19.587
22	19.827	20.070	20.316	20.565	20.815
23	21.068	21.324	21.583	21.845	22.110
24	22.377	22.648	22.922	23.198	23.476
25	23.756	24.039	24.326	24.617	24.912
26	25.209	25.509	25.812	26.117	26.426
27	26.739	27.055	27.734	27.696	28.021
28	28.349	28.680	29.015	29.354	29.697
29	30.043	30.392	30.745	31.102	31.461
30	31.824	32.191	32.561	32.934	33.312

APPENDIX 5. Line drawings of seismic profiles.

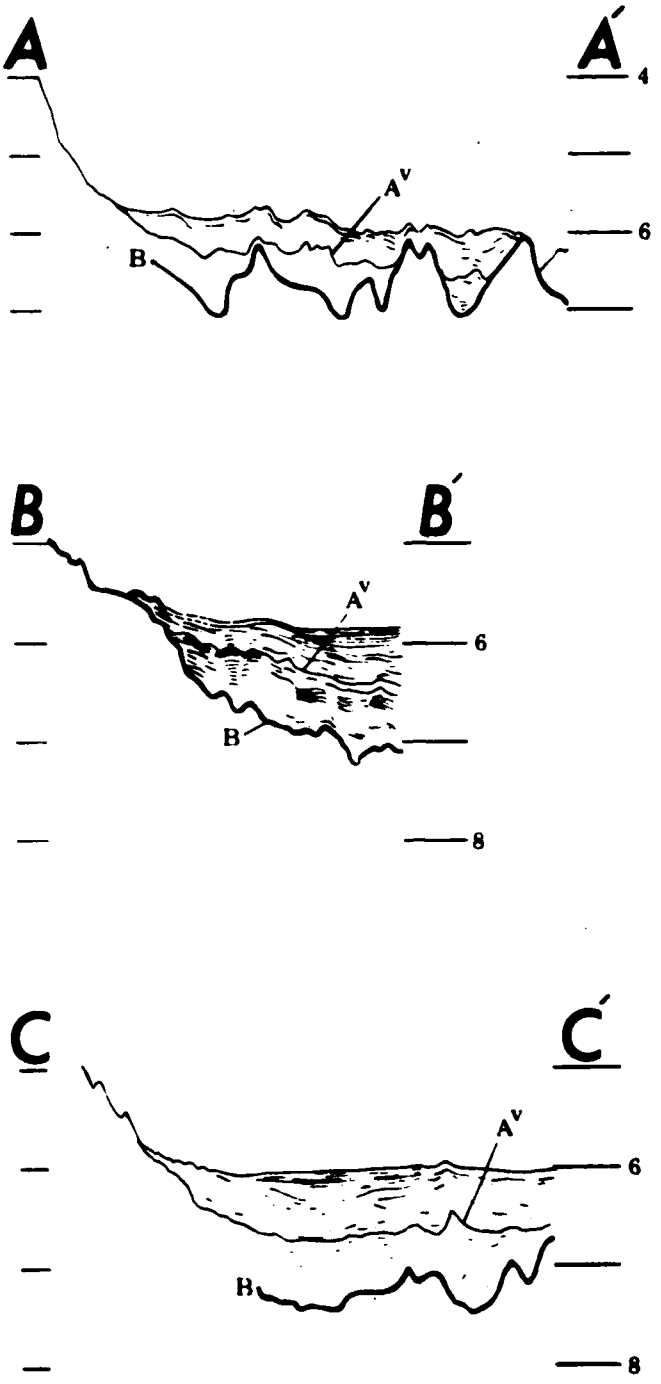

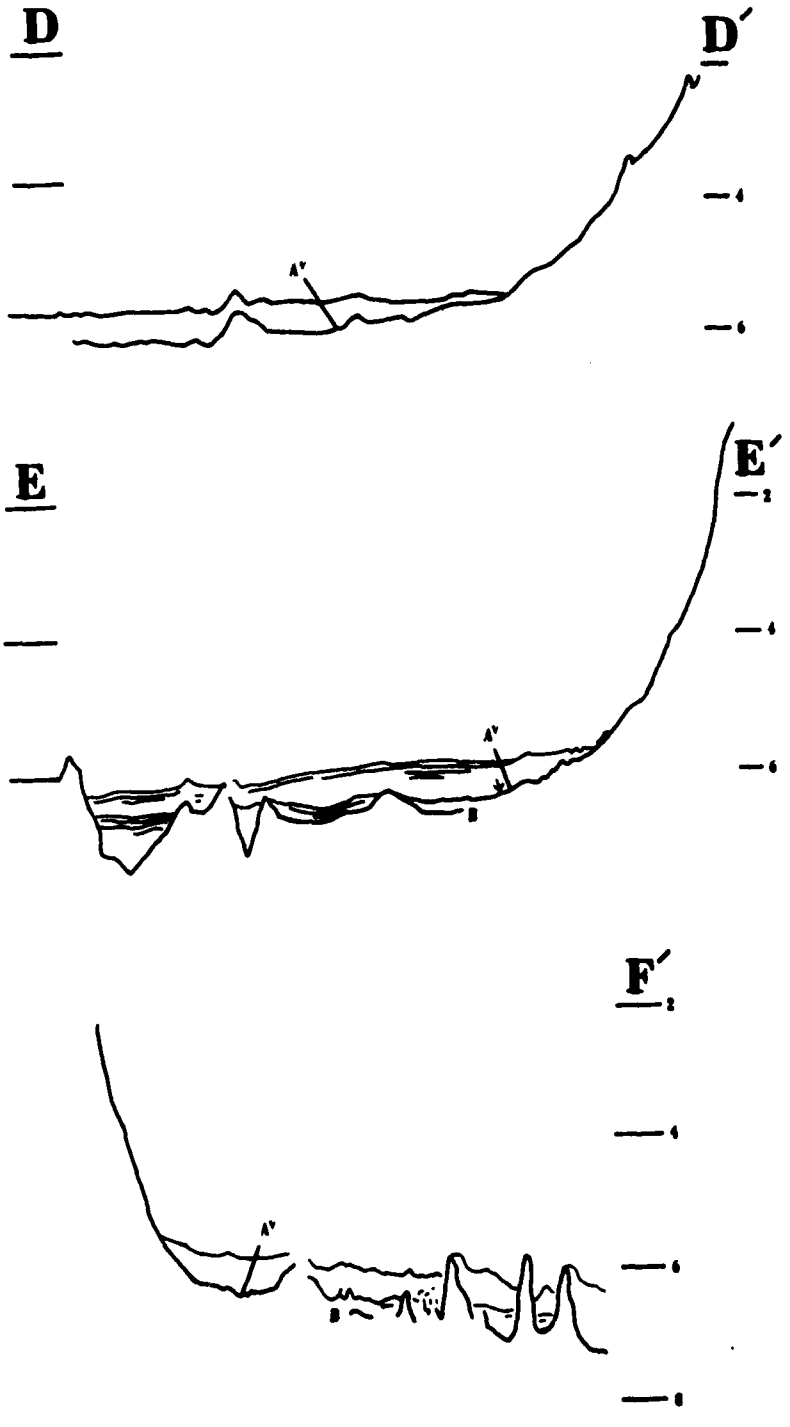
D
D´
E
E´
F´

APPENDIX 6. Clay mineral content of V7-65; X-ray pattern.

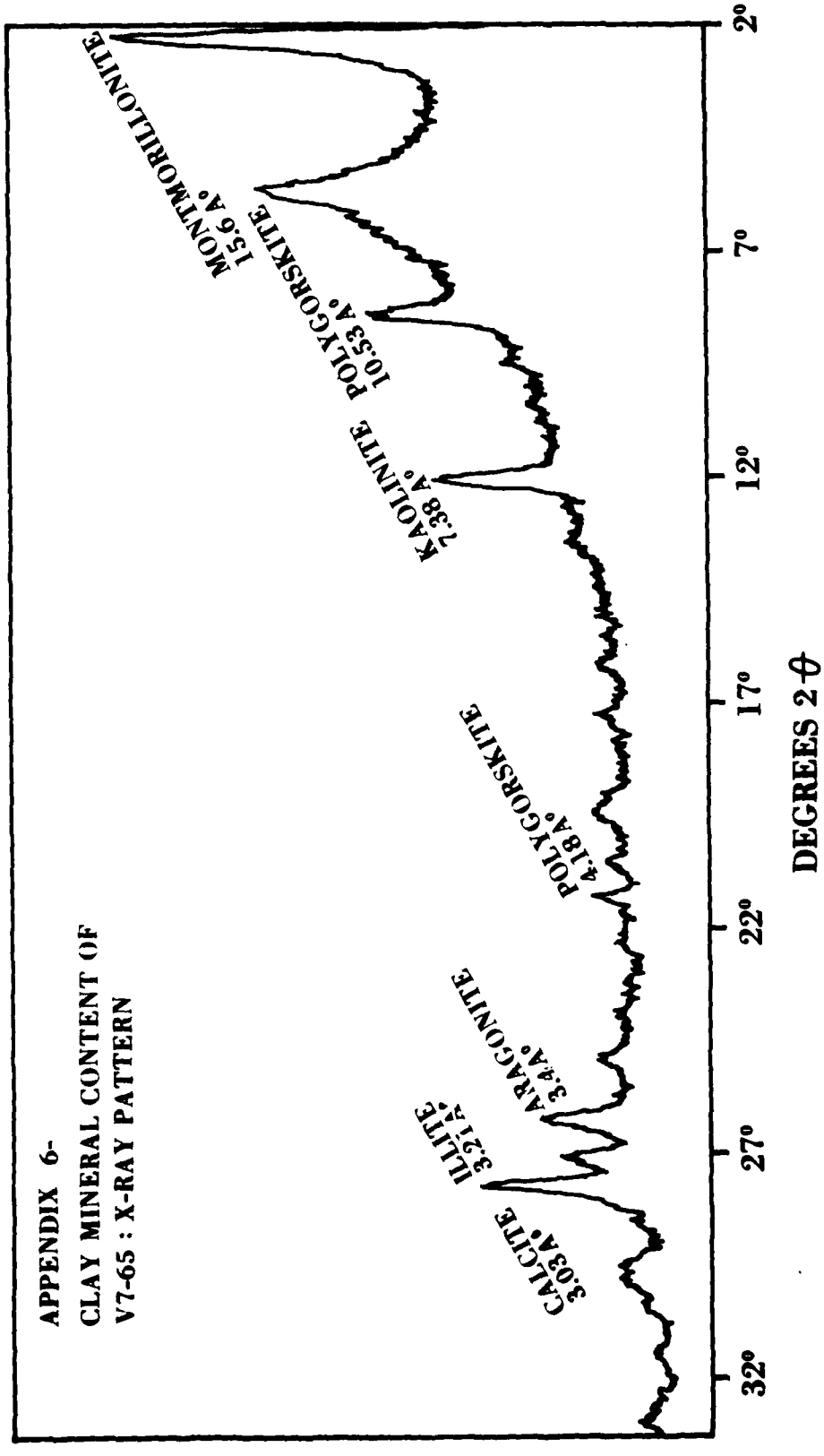

APPENDIX 7. Grain size distributions for the top, 10, 20, and 30 cm intervals of all the pedestal cores.

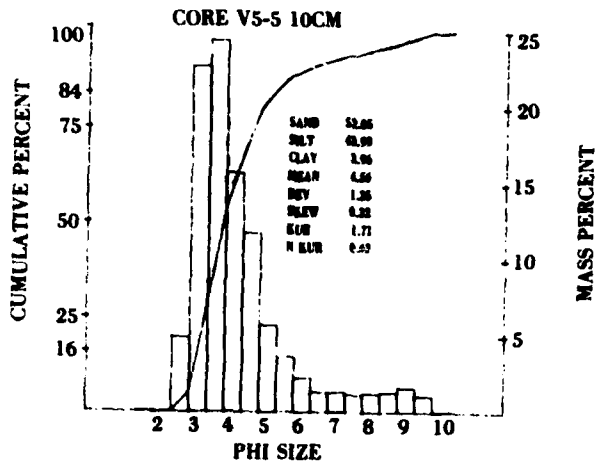

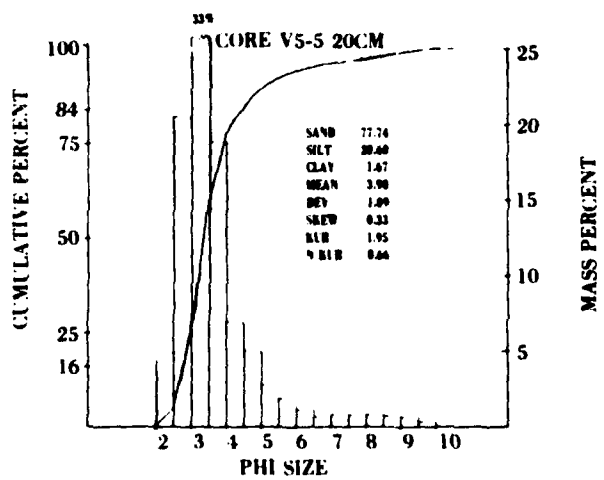

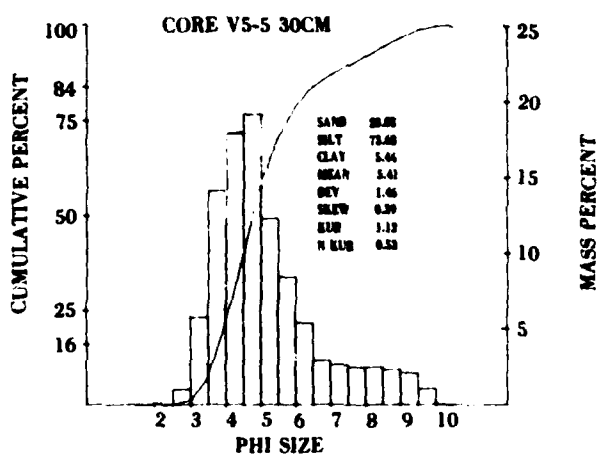

AD-A126 871 SEDIMENTS ON THE SOUTHEASTERN FLANK OF THE BERMUDA PEDESTAL(U) NAVAL OCEAN RESEARCH AND DEVELOPMENT ACTIVITY NSTL STATION MS D LAVOIE ET AL. MAR 83 2/2

UNCLASSIFIED NORDA-TN-198 F/G 8/10 NL

END
DATE FILMED
5 83
DTIC

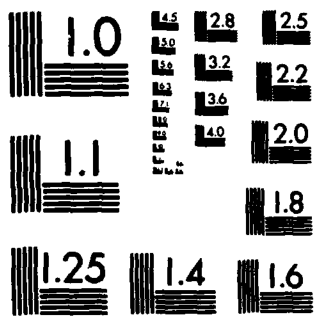

MICROCOPY RESOLUTION TEST CHART
NATIONAL BUREAU OF STANDARDS-1963-A

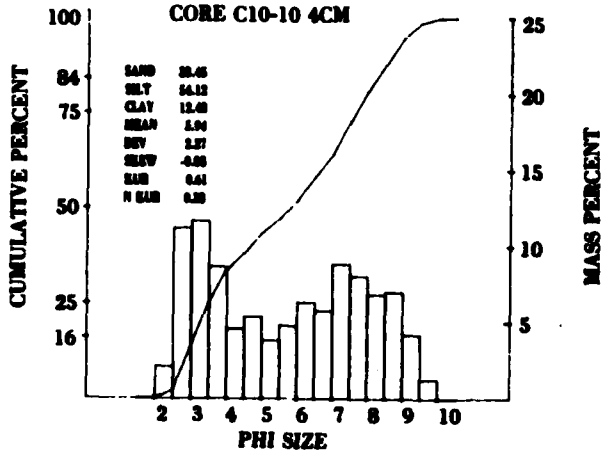
CORE C10-10 4CM
CUMULATIVE PERCENT
MASS PERCENT
PHI SIZE
100
84
75
50
25
16
25
20
15
10
5
2 3 4 5 6 7 8 9 10

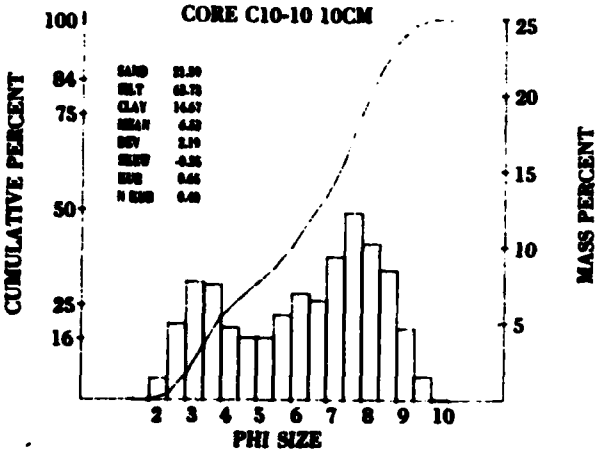
CORE C10-10 10CM
CUMULATIVE PERCENT
MASS PERCENT
PHI SIZE
100
84
75
50
25
16
25
20
15
10
5
2 3 4 5 6 7 8 9 10

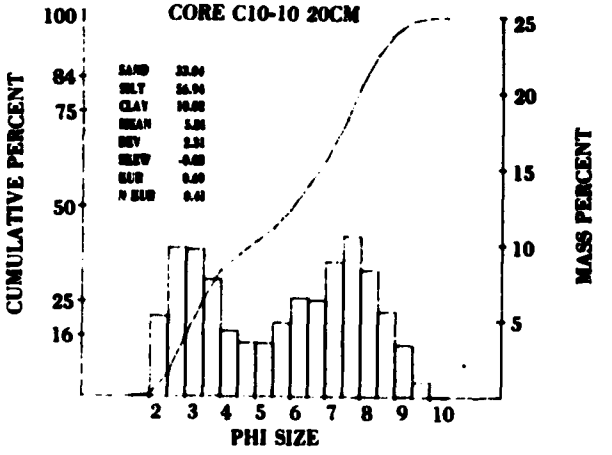
CORE C10-10 20CM
CUMULATIVE PERCENT
MASS PERCENT
PHI SIZE
100
84
75
50
25
16
25
20
15
10
5
2 3 4 5 6 7 8 9 10

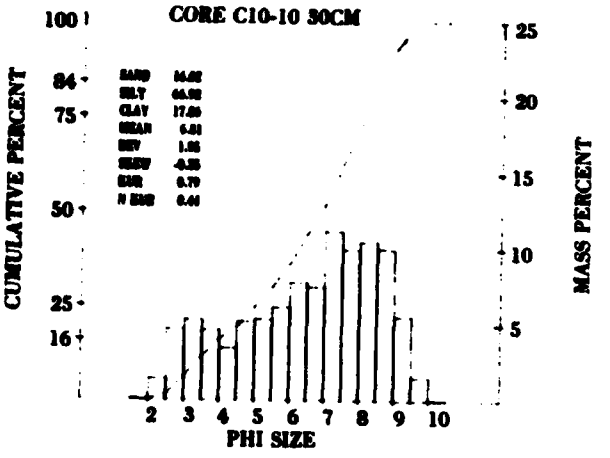
CORE C10-10 30CM
CUMULATIVE PERCENT
MASS PERCENT
PHI SIZE
100
84
75
50
25
16
25
20
15
10
5
2 3 4 5 6 7 8 9 10

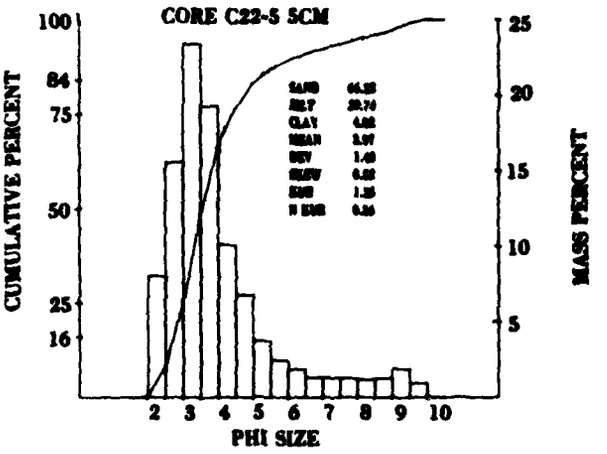
CORE C22-5 5CM
CUMULATIVE PERCENT
MASS PERCENT
PHI SIZE
100
84
75
50
25
16
25
20
15
10
5
2 3 4 5 6 7 8 9 10

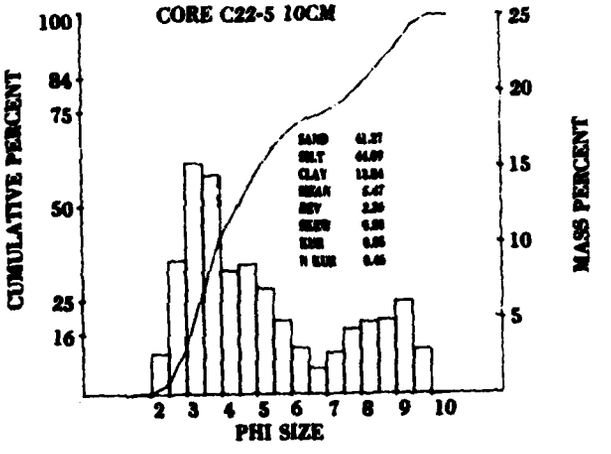
CORE C22-5 10CM
CUMULATIVE PERCENT
MASS PERCENT
PHI SIZE
100
84
75
50
25
16
25
20
15
10
5
2 3 4 5 6 7 8 9 10

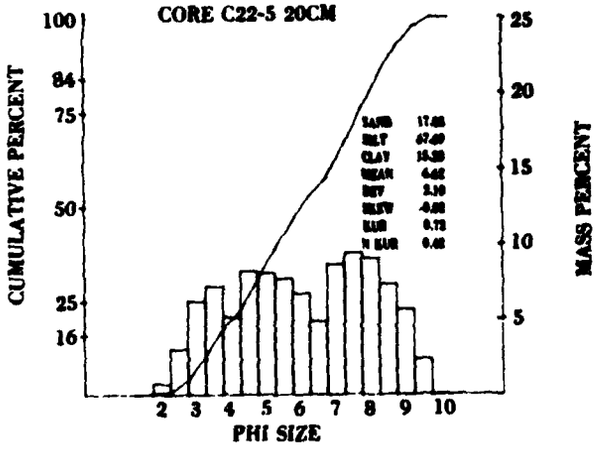
CORE C22-5 20CM
CUMULATIVE PERCENT
MASS PERCENT
PHI SIZE
100
84
75
50
25
16
25
20
15
10
5
2 3 4 5 6 7 8 9 10

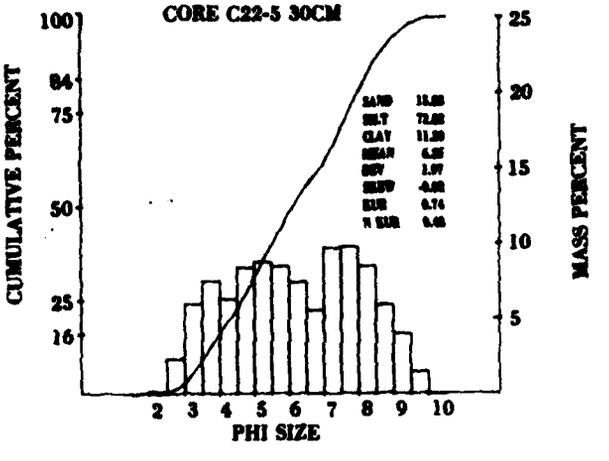
CORE C22-5 30CM
CUMULATIVE PERCENT
MASS PERCENT
PHI SIZE
100
84
75
50
25
16
25
20
15
10
5
2 3 4 5 6 7 8 9 10

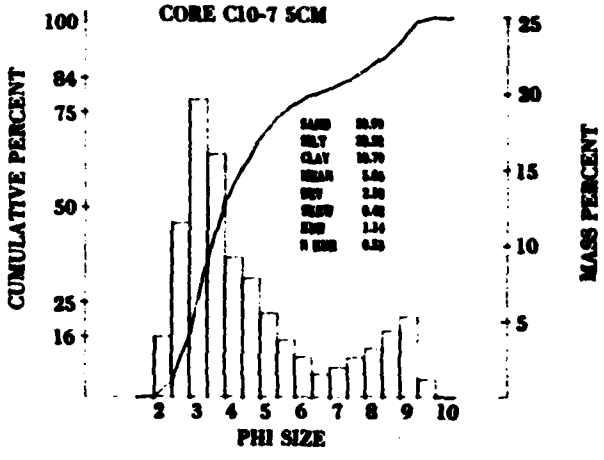
CORE C10-7 5CM
CUMULATIVE PERCENT
MASS PERCENT
PHI SIZE
100
84
75
50
25
16
25
20
15
10
5
2 3 4 5 6 7 8 9 10

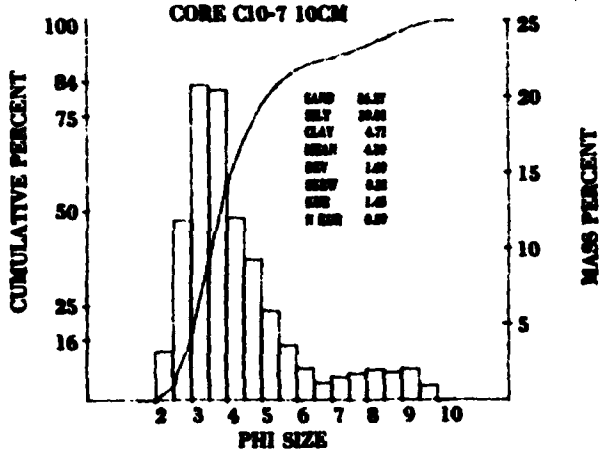
CORE C10-7 10CM
CUMULATIVE PERCENT
MASS PERCENT
PHI SIZE
100
84
75
50
25
16
25
20
15
10
5
2 3 4 5 6 7 8 9 10

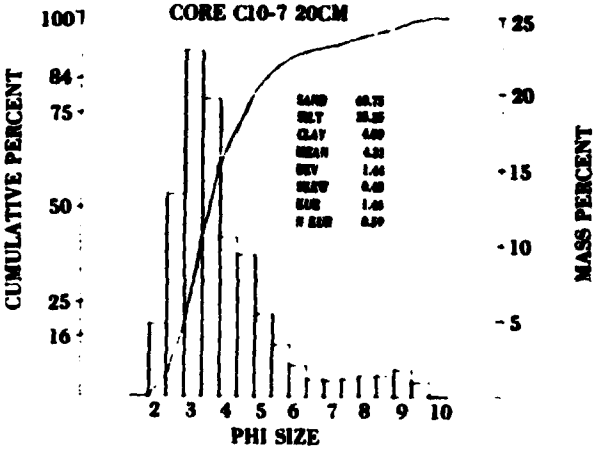
CORE C10-7 20CM
CUMULATIVE PERCENT
MASS PERCENT
PHI SIZE
100
84
75
50
25
16
25
20
15
10
5
2 3 4 5 6 7 8 9 10

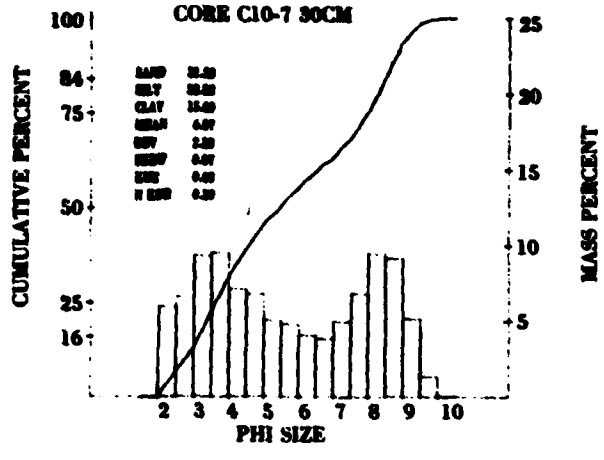
CORE C10-7 30CM
CUMULATIVE PERCENT
MASS PERCENT
PHI SIZE
100
84
75
50
25
16
25
20
15
10
5
2 3 4 5 6 7 8 9 10

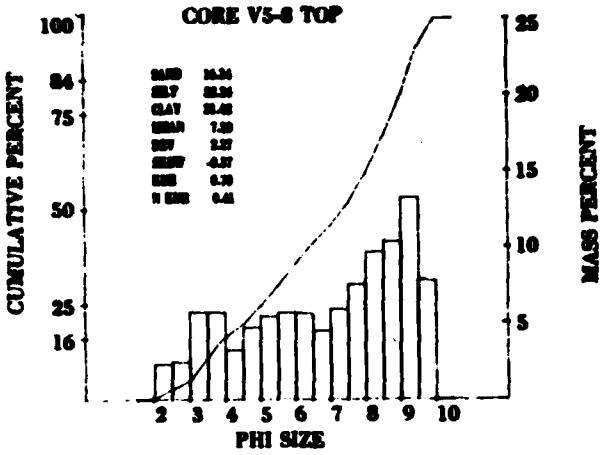
CORE V5-8 TOP
CUMULATIVE PERCENT
MASS PERCENT
PHI SIZE
100
84
75
50
25
16
25
20
15
10
5
2 3 4 5 6 7 8 9 10

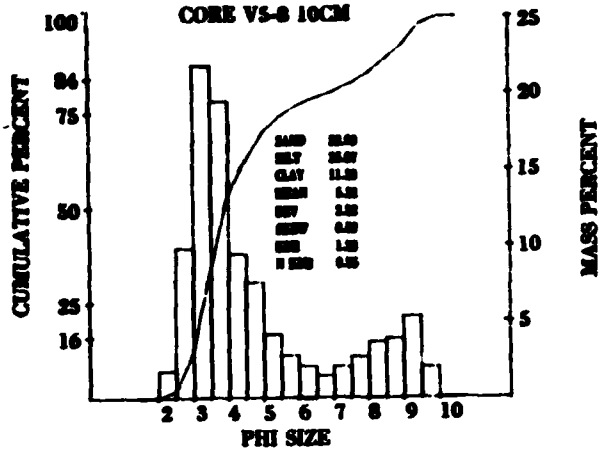
CORE V5-8 10CM
CUMULATIVE PERCENT
MASS PERCENT
PHI SIZE
100
84
75
50
25
16
25
20
15
10
5
2 3 4 5 6 7 8 9 10

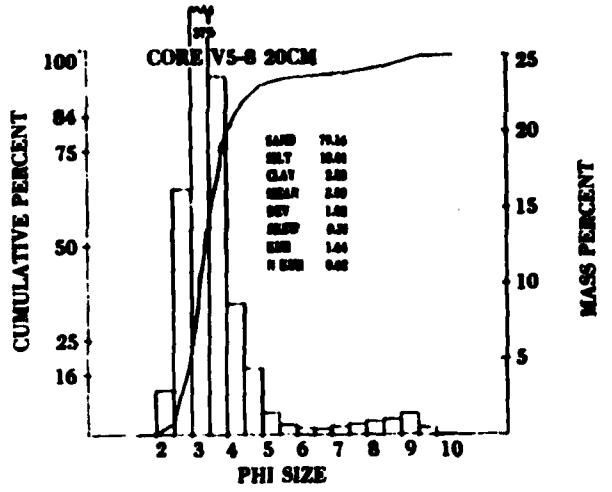
CORE V5-8 20CM
CUMULATIVE PERCENT
MASS PERCENT
PHI SIZE
100
84
75
50
25
16
25
20
15
10
5
2 3 4 5 6 7 8 9 10

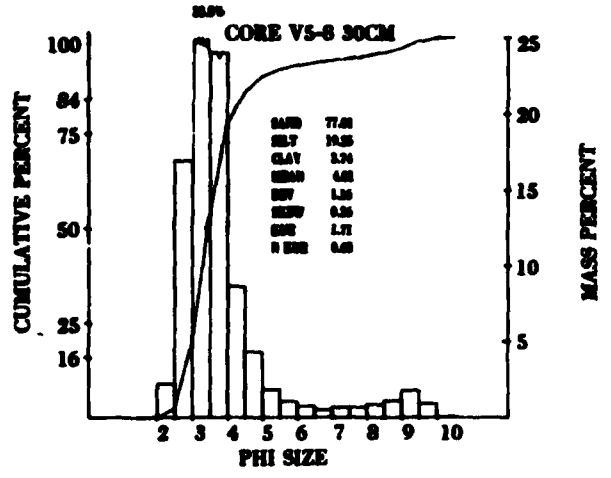
CORE V5-8 30CM
CUMULATIVE PERCENT
MASS PERCENT
PHI SIZE
100
84
75
50
25
16
25
20
15
10
5
2 3 4 5 6 7 8 9 10

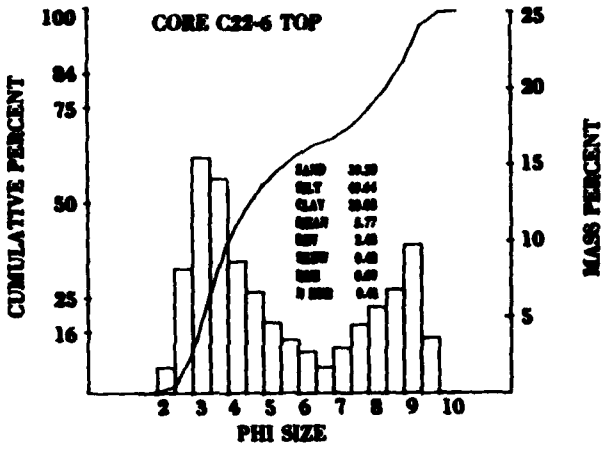
CORE C22-6 TOP
CUMULATIVE PERCENT
MASS PERCENT
PHI SIZE
100
84
75
50
25
16
25
20
15
10
5
2 3 4 5 6 7 8 9 10

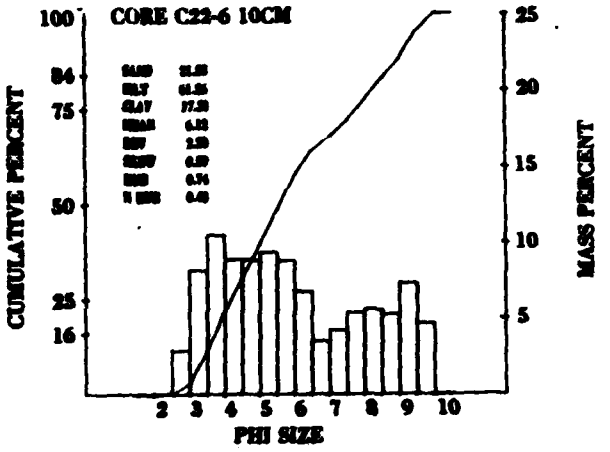
CORE C22-6 10CM
CUMULATIVE PERCENT
MASS PERCENT
PHI SIZE
100
84
75
50
25
16
25
20
15
10
5
2 3 4 5 6 7 8 9 10

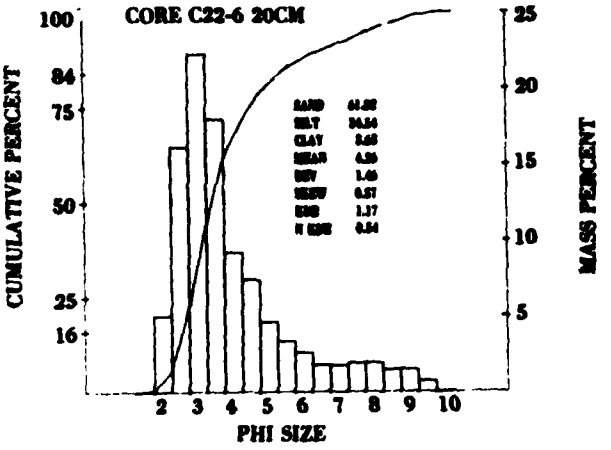
CORE C22-6 20CM
CUMULATIVE PERCENT
MASS PERCENT
PHI SIZE
100
84
75
50
25
16
25
20
15
10
5
2 3 4 5 6 7 8 9 10

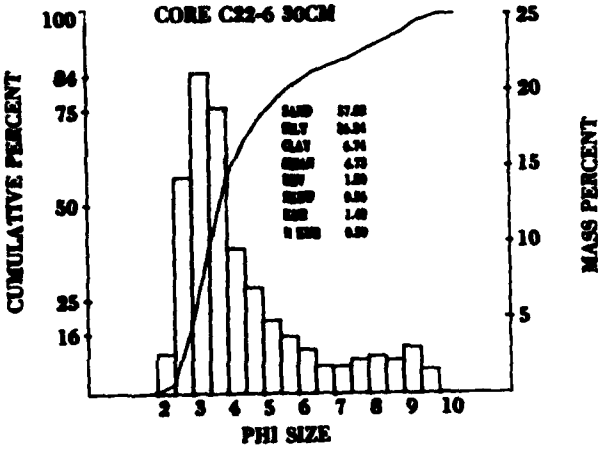
CORE C22-6 30CM
CUMULATIVE PERCENT
MASS PERCENT
PHI SIZE
100
84
75
50
25
16
25
20
15
10
5
2 3 4 5 6 7 8 9 10

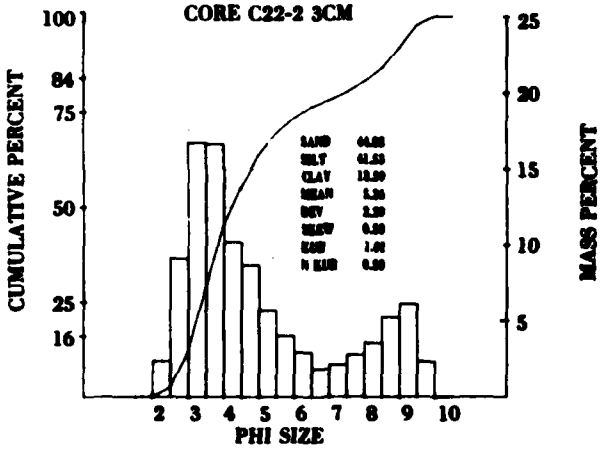
CORE C22-2 3CM
CUMULATIVE PERCENT
MASS PERCENT
PHI SIZE
100
84
75
50
25
16
25
20
15
10
5
2 3 4 5 6 7 8 9 10

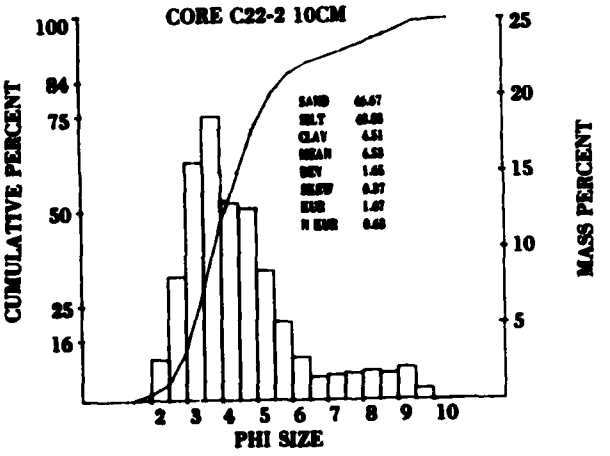
CORE C22-2 10CM
CUMULATIVE PERCENT
MASS PERCENT
PHI SIZE
100
84
75
50
25
16
25
20
15
10
5
2 3 4 5 6 7 8 9 10

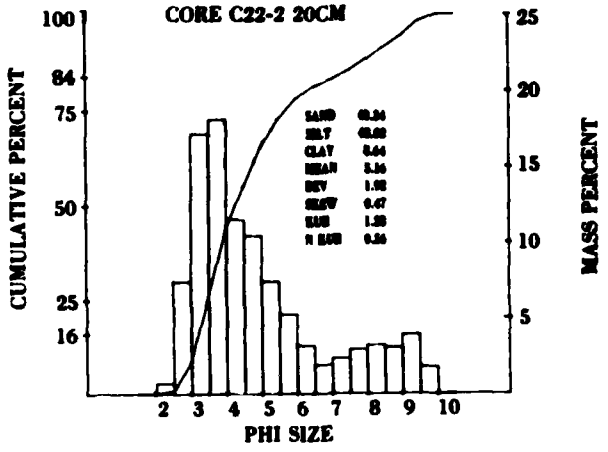
CORE C22-2 20CM
CUMULATIVE PERCENT
MASS PERCENT
PHI SIZE
100
84
75
50
25
16
25
20
15
10
5
2 3 4 5 6 7 8 9 10

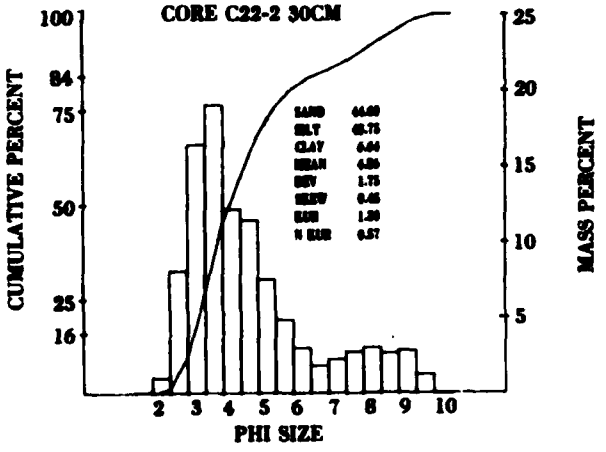
CORE C22-2 30CM
CUMULATIVE PERCENT
MASS PERCENT
PHI SIZE
100
84
75
50
25
16
25
20
15
10
5
2 3 4 5 6 7 8 9 10

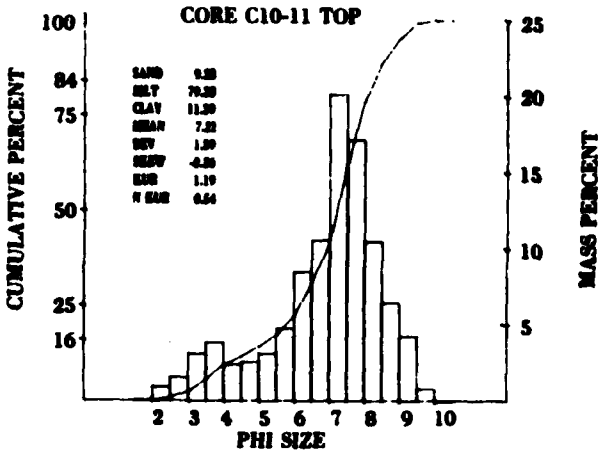
CORE C10-11 TOP
CUMULATIVE PERCENT
MASS PERCENT
PHI SIZE
100
84
75
50
25
16
25
20
15
10
5
2 3 4 5 6 7 8 9 10

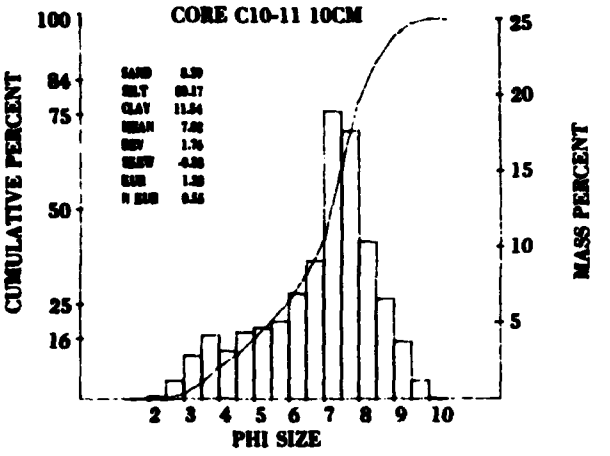
CORE C10-11 10CM
CUMULATIVE PERCENT
MASS PERCENT
PHI SIZE
100
84
75
50
25
16
25
20
15
10
5
2 3 4 5 6 7 8 9 10

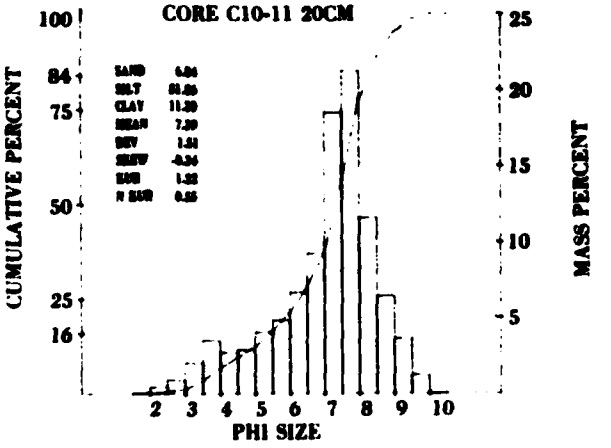
CORE C10-11 20CM
CUMULATIVE PERCENT
MASS PERCENT
PHI SIZE
100
84
75
50
25
16
25
20
15
10
5
2 3 4 5 6 7 8 9 10

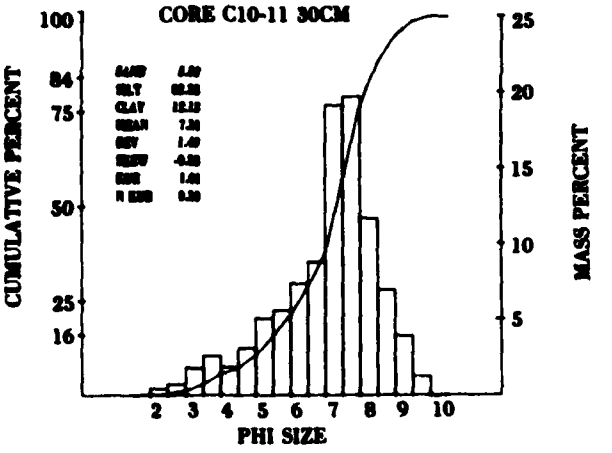
CORE C10-11 30CM
CUMULATIVE PERCENT
MASS PERCENT
PHI SIZE
100
84
75
50
25
16
25
20
15
10
5
2 3 4 5 6 7 8 9 10

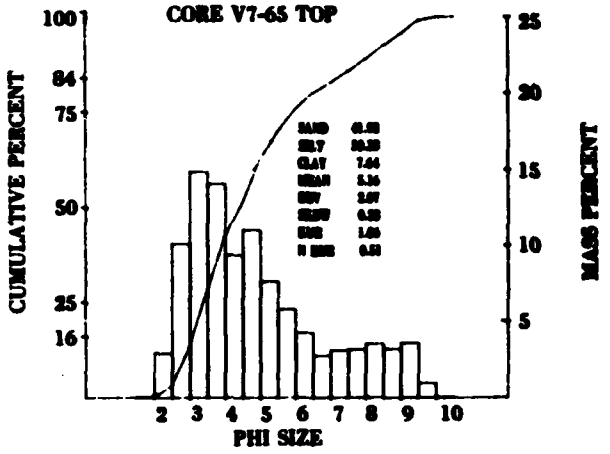
CORE V7-65 TOP
CUMULATIVE PERCENT
MASS PERCENT
PHI SIZE
100
84
75
50
25
16
25
20
15
10
5
2 3 4 5 6 7 8 9 10

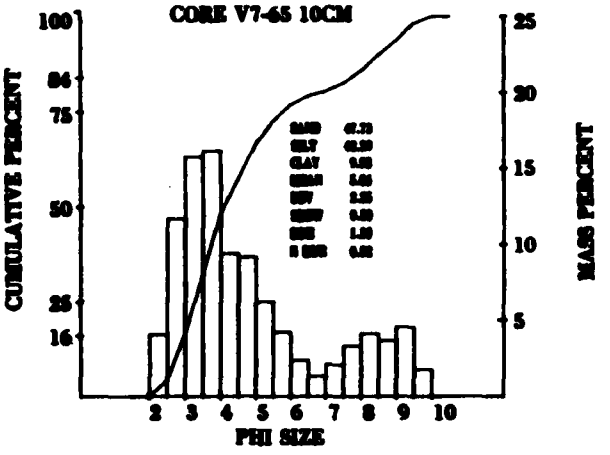
CORE V7-65 10CM
CUMULATIVE PERCENT
MASS PERCENT
PHI SIZE
100
84
75
50
25
16
25
20
15
10
5
2 3 4 5 6 7 8 9 10

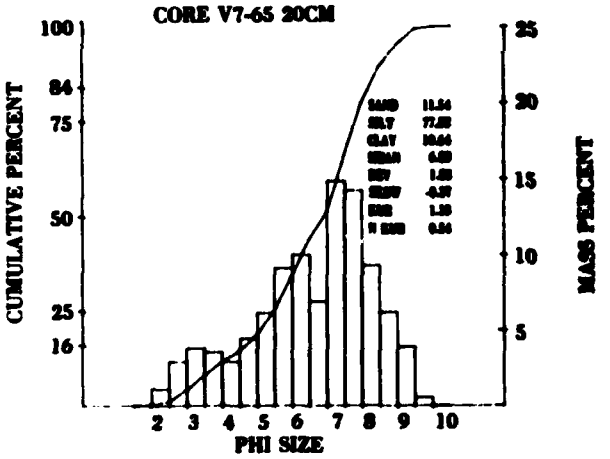
CORE V7-65 20CM
CUMULATIVE PERCENT
MASS PERCENT
PHI SIZE
100
84
75
50
25
16
25
20
15
10
5
2 3 4 5 6 7 8 9 10

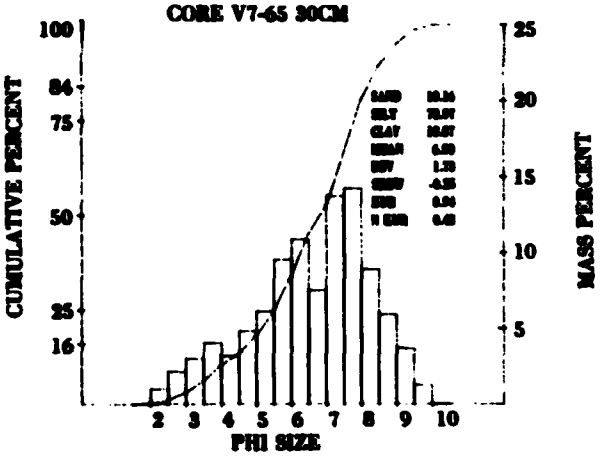
CORE V7-65 30CM
CUMULATIVE PERCENT
MASS PERCENT
PHI SIZE
100
84
75
50
25
16
25
20
15
10
5
2 3 4 5 6 7 8 9 10

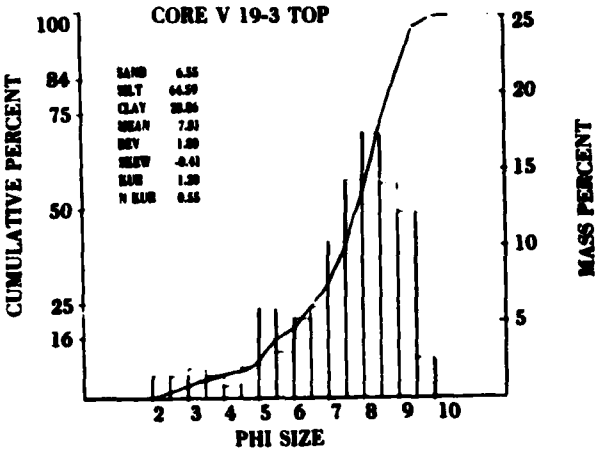
CORE V 19-3 TOP
CUMULATIVE PERCENT
MASS PERCENT
PHI SIZE
100
84
75
50
25
16
25
20
15
10
5
2 3 4 5 6 7 8 9 10

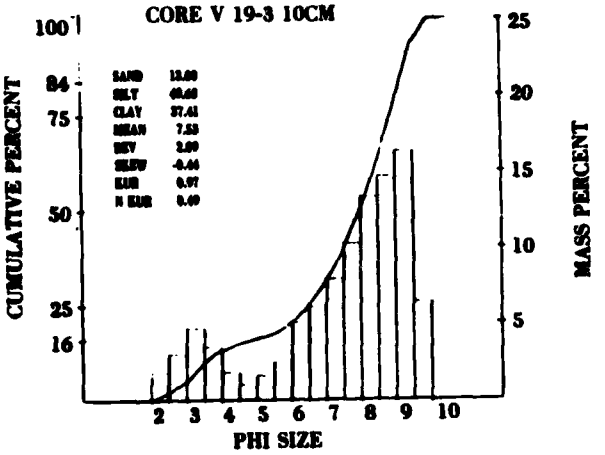
CORE V 19-3 10CM
CUMULATIVE PERCENT
MASS PERCENT
PHI SIZE
100
84
75
50
25
16
25
20
15
10
5
2 3 4 5 6 7 8 9 10

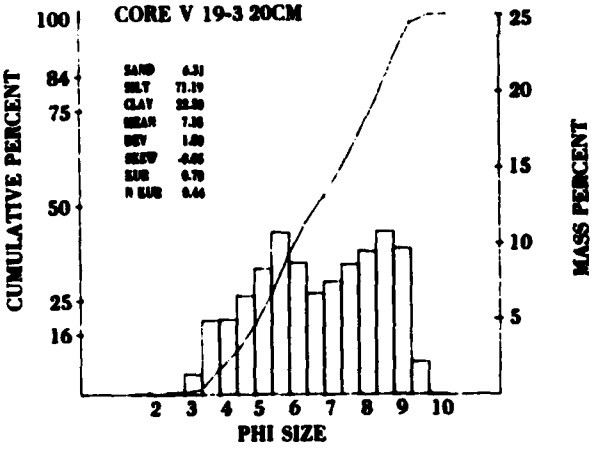
CORE V 19-3 20CM
CUMULATIVE PERCENT
MASS PERCENT
PHI SIZE
100
84
75
50
25
16
25
20
15
10
5
2 3 4 5 6 7 8 9 10

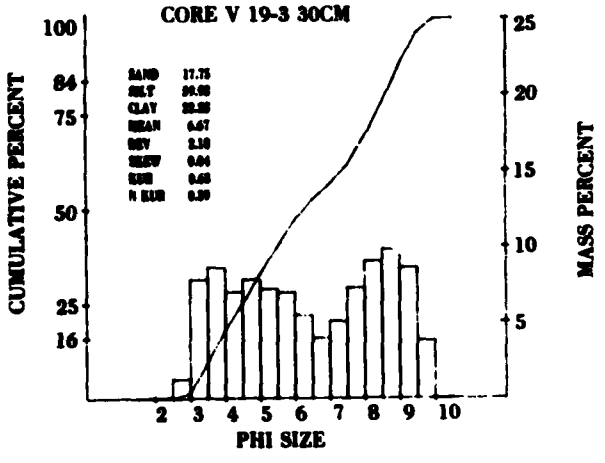
CORE V 19-3 30CM
CUMULATIVE PERCENT
MASS PERCENT
PHI SIZE
100
84
75
50
25
16
25
20
15
10
5
2 3 4 5 6 7 8 9 10

UNCLASSIFIED

SECURITY CLASSIFICATION OF THIS PAGE (When Data Entered)

REPORT DOCUMENTATION PAGE		READ INSTRUCTIONS BEFORE COMPLETING FORM
1. REPORT NUMBER NORDA Technical Note 198 AD-A12687	2. GOVT ACCESSION NO.	3. RECIPIENT'S CATALOG NUMBER 1
4. TITLE (and Subtitle) Sediments on the Southeastern Flank of the Bermuda Pedestal		5. TYPE OF REPORT & PERIOD COVERED 6. PERFORMING ORG. REPORT NUMBER
7. AUTHOR(s) Dawn Lavoie James E. Matthews		8. CONTRACT OR GRANT NUMBER(s)
9. PERFORMING ORGANIZATION NAME AND ADDRESS Naval Ocean Research and Development Activity NSTL Station, Mississippi 39529		10. PROGRAM ELEMENT, PROJECT, TASK AREA & WORK UNIT NUMBERS 62759N
11. CONTROLLING OFFICE NAME AND ADDRESS Naval Ocean Research and Development Activity NSTL Station, Mississippi 39529		12. REPORT DATE March 1983 13. NUMBER OF PAGES 104
14. MONITORING AGENCY NAME & ADDRESS(if different from Controlling Office)		15. SECURITY CLASS. (of this report) UNCLASSIFIED 15a. DECLASSIFICATION/DOWNGRADING SCHEDULE

16. DISTRIBUTION STATEMENT (of this Report)

Distribution Unlimited

17. DISTRIBUTION STATEMENT (of the abstract entered in Block 20, if different from Report)

18. SUPPLEMENTARY NOTES

19. KEY WORDS (Continue on reverse side if necessary and identify by block number)

Geology
Seamounts

20. ABSTRACT (Continue on reverse side if necessary and identify by block number)

The Bermuda Pedestal is a truncated, flat-topped, volcanic cone located in the western North Atlantic Ocean at approximately 32°20'N and 64°45'W. The pedestal has steep slopes ranging from 30° near the top to 2.5° near the bottom. Seismic records indicate sparse sediment cover on the slopes and an absence of large amounts of slump material on the lower slopes of the pedestal. This suggests that the apron at the base is not recent; rather, it may be a remnant of a talus slope associated with mid Eocene-Oligocene volcanic and erosional events. (over)

DD FORM 1 JAN 73 1473 EDITION OF 1 NOV 6[illegible] OBSOLETE
S/N 0[illegible]

UNCLASSIFIED

SECURITY CLASSIFICATION OF THIS PAGE (When Data Entered)

(continued from Block 20)

The carbonate content of surface and near-surface sediment (quaternary) is generally high, decreasing only slightly with increasing depth in spite of probable extensive dissolution. Carbonate constituents are composed of both shallow platform and pelagic organisms. Constituent particles identified by scanning electron microscopy correlate well in most instances with mineralogy identified by X-ray diffraction. Clay mineral content is low to nonexistent on the pedestal. In general, grain sizes tend to be coarser near the top of the pedestal, but anomalously high percentages of sand were found in a few places low on the flank and apron of the pedestal.

Sediment deposition on the pedestal is discontinuous and episodic, a combination of pelagic "rain" and redeposition by rapid-transport processes such as slumping, turbidity currents, and resuspension and dispersion of sediment by eddies and currents.

F

5